 doi:10.20944/preprints201803.0273.v1

applied sciences

MDPI

Type of the Paper (Review)

Resolution Enhancement in Phase Microscopy: a Review

Juanjuan Zheng [1], Vicente Micó [2,*], Peng Gao [1, 3, 4,*]

[1] School of Physics and Optoelectronic Engineering, Xidian University, Xi'an, 710071, China
[2] Departamento de Óptica y de Optometría y Ciencias de la Visión, Universitat de Valencia, C/Doctor Moliner 50, Burjassot 46100, Spain
[3] Institute of Applied Physics, Karlsruhe Institute of Technology, 76131 Karlsruhe, Germany
[4] Institute of Nanotechnology, Karlsruhe Institute of Technology, 76344 Eggenstein-Leopoldshafen, Germany
* Correspondence: vicente.mico@uv.es (VM) and peng.gao@kit.edu (PG);

Abstract: Quantitative phase microscopy (QPM), a technique combining phase imaging and microscopy, enables visualization of the 3-D topography in reflective samples as well as the inner structure or refractive index distribution of transparent and translucent samples. However, as in conventional optical microscopy, QPM provides either a large field of view (FOV) or a high resolution but not both. Many approaches such as oblique illumination, structured illumination and speckle illumination have been proposed to improve the spatial resolution of phase microscopy by restricting other degrees of freedom (mostly time). Therefore, the space bandwidth product (SBP) of QPM becomes enlarged. This paper aims to provide an up-to-date review on the resolution enhancement approaches of QPM, discussing the pros and cons of each technique as well as the confusion on resolution definition claim on QPM and other coherent microscopy.

Keywords: Quantitative phase microscopy; Digital holographic microscopy; lensless microscopy; resolution enhancement; space bandwidth product

1. Introduction

Despite other high-resolution microscopy technologies, e.g., scanning electron microscopy (SEM), scanning tunnel microscopy (STM) and atomic force microscopy (AFM), optical microscopy acts as a mainstream inspection tool in the imaging community, especially, in biological studies. The main reason is because optical microscopy is a minimally invasive technique and therefore compatible to live cell or tissue. When being used with fluorescence specific labeling strategy, a certain kind of biomolecule on targeted structures can be observed. However, due to the diffraction-limit imposed by the wave nature of light, conventional optical microscopy has a spatial resolution around half of the used wavelength (typically ~200 nm) and thus, cannot resolve the subcellular structures finer than this limit. Since the 90s of the 20th Century, this limitation has been broken by the development of super-resolution optical microscopy [1-3]. The key of super-resolution microscopy is to switch single molecules "on" and "off" by light and therefore, a high-resolution image can be described by these single molecules.

There is no doubt that the usage of fluorescence markers has revolutionary advantages since it enables observation of specific targeted molecules. Nevertheless, it is also desirable to directly observe cells or tissues for their morphological structures in their natural condition, since fluorescence probes are harmful, or at least of disturbance, to biological systems. Of note, the determination of the 3-D shape and refractive index of biological samples has recently experienced a

 doi:10.20944/preprints201803.0273.v1

growing interest in the biomedical community [4-6]. However, looking directly at biological samples is tremendously challenging since they are transparent or translucent under the visible light. Luckily, when a light propagates through a cell, its phase is distorted as consequence of the thickness profile and the refractive index distribution of the cell. And this information can be exploited to visualize (qualitative imaging) and characterize (quantitative imaging) those transparent samples.

There are many approaches to retrieve the phase information of a sample. Wavefront sensing, employing a Shack-Hartmann sensor [7] or a pyramid sensor [8], is a simple and useful approach to investigate slightly distorted wavefronts. The basic idea is to spatially divide the tested wavefront into a series of sub-regions and focus them separately onto a CCD camera typically with a micro-lens array. Then, by analyzing the location of the spots on the CCD, the local slope of the wavefront over each region is computed. Besides wavefront sensors, interferometric approaches are the most commonly used techniques to retrieve phase information. Here, a reference wave is superimposed to the object wave and the phase is reconstructed from the generated interference pattern [9-27]. Alternatively, beam-propagation-based methods can also retrieve the phase distribution by recording a series of diffraction patterns under different conditions or applying different perturbations [28-36]. For example, a diffracted beam by a phase sample influences the propagation of the beam and results in different intensity distributions at different planes. Vice versa, the phase can be recovered by analyzing the intensity distributions of a diffracted beam recorded at different distances [28] or by using different illumination wavelengths [33-36].

Quantitative phase microscopy (QPM) emerges as a combination between phase imaging and microscopy. Thus, QPM has similar constraints than conventional optical microscopy regarding basic properties such as resolving power, available field of view (FOV), working distance, depth of focus and global costs. Of special interest are the spatial resolution limit and the FOV provided by QPM which directly come from the used microscope lens and that are closely related one to each other since the higher the former, the lower the latter (and vice versa). The ratio between these two parameters defines the space-bandwidth product (SBP) degree of freedom of the QPM imaging system [37]. The SBP concept generalizes the theorem of invariance of information capacity [38] because not only degrees of freedom are considered but also the shape of the SPB of the imaging system. Just as an example, a standard 20X microscope lens with a resolution limit of 0.8 μm and a circular FOV of 1.1 mm in diameter, provides a SBP of ~7 megapixels [39]. However, microscopists always expect to have higher SBP in the sense of increasing resolution while maintaining FOV or, in other words, to provide enhanced resolution under the same FOV. This can be accomplished from a theoretical point of view by matching the SBP of the sample with the SBP of the imaging system in order to allow effective transmission range of the sample's image through the microscope system [40,41].

In the past decades, there were many efforts to improve spatial resolution without scarifying the FOV size. This paper aims to complete and update previous manuscripts dealing with overviews about superresolution [42,43] by providing an up-to-date review on the approaches to enhance the resolution in QPM. Moreover, it includes an overview about enhanced resolution in lensless QPM. This paper will also cover the pros and cons of each technique, as well as the confusion on resolution definition claim on QPM and other coherent microscopy techniques. This article is organized as follows: Section 2 summarizes the applications of QPM; Section 3 reviews resolution enhancement approaches in lens-based interferometric QPM; Section 4 overviews resolution enhancement approaches in lensless interferometric QPM; Section 5 presents resolution enhancement approaches of reference-less QPM. Section 6 describes the criterion for evaluating the resolution of QPM; Finally, Section 7 summarizes this review.

2. Quantitative Phase Microscopy (QPM) and its Applications

When a beam is reflected by the sample's surface or passes through a transparent sample, the phase of the beam contains information about, respectively, the 3-D sample's profile or the refractive index

Preprints (www.preprints.org) | NOT PEER-REVIEWED | Posted: 30 March 2018 doi:10.20944/preprints201803.0273.v1

distribution of the sample. This information can be exploited thus providing not only high-contrast images of transparent samples (qualitative improvement), but also quantitative evaluation on their 3-D profiles or refractive index distributions [44]. In that sense, QPM provides a versatile tool to observe or investigate the microscopic world quantitatively. Hence, QPM has been widely used in industrial inspection [11,45], biomedical observation [46-50], special beam generation [51-54], air or liquid flow monitoring [55,56], and adaptive imaging [57]. Figure 1 summarizes some of these applications.

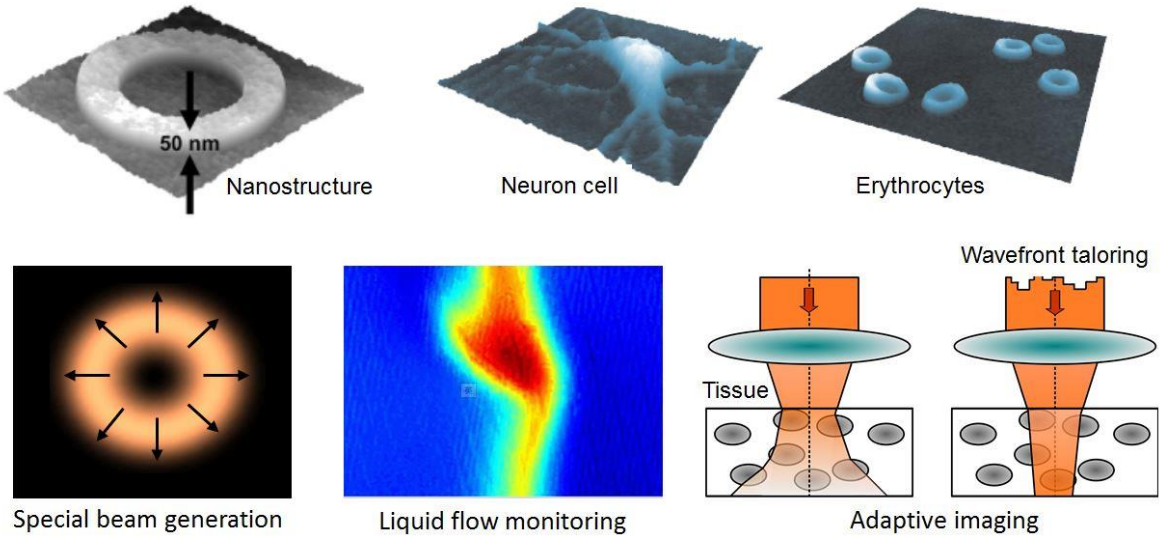

Figure 1. Applications of QPM. The three images on the top are adapted from Ref. [11]

In conventional bright field microscopy, illumination is provided by an incoherent source (such as a thermal light) and the diffraction-limited resolution is defined as $\delta_{min}=0.61\lambda/NA$ where λ and NA indicate the illumination wavelength and the numerical aperture of the objective lens. However, in QPM, a coherent or partially-coherent light is used for illumination and the resolution limit becomes in $\delta_{min}=0.82\lambda/NA$ [58,59] (*vide infra*, section 5). This limit can be improved by using shorter illumination wavelengths [60,61], or by synthesizing a larger numerical aperture [62-65] using different illumination strategies such as oblique illumination (see Ref. [42] for an extensive reference list on synthetic aperture generation by tilted beam illumination), structured illumination [32,66-71], grating projection [72-75], and illuminating with random patterns [76-81]. Depending on whether a reference wave is needed or not in QPM, these resolution enhancement approaches can be categorized into two groups: Resolution enhanced QPM via interferometric approaches and Resolution enhanced by single-beam QPM.

3. Resolution enhancement approaches in lens-based DHM

The background layout for interferometric QPM is defined by digital holographic microscopy (DHM). Figure 2 presents a typical DHM setup in transmission mode where the architecture is based on a standard Mach-Zehnder interferometer. The laser output is split into the object and reference waves by the beam splitter BS_1. In the object wave path, the beam is expanded by the beam expander BE_1 and illuminates a sample located in the front focal plane of the objective MO. After passing through

Preprints (www.preprints.org) | NOT PEER-REVIEWED | Posted: 30 March 2018 doi:10.20944/preprints201803.0273.v1

the specimen, the object wave curvature is magnified by the MO and collimated by the lens L before reaching the digital sensor. This object wave interferes with the reference wave which is also expanded by a second beam expander BE_2 in order to equalize beam curvature. Both beams generate hologram (Figure. 2(b)) which is recorded by a charge-coupled device (CCD) or complementary metal–oxide–semiconductor (CMOS). After digitally reconstruction from the recorded hologram [9,11,12,56], the complex amplitude distribution (intensity and phase) of the sample is recovered (Figures 2(c, d)). Unlike conventional microscope which only provides in-focus sample images, DHM does not need an image plane hologram to achieve imaging since it is capable of digitally refocus the sample afterwards [13,21,82-84] by using numerical propagation tools.

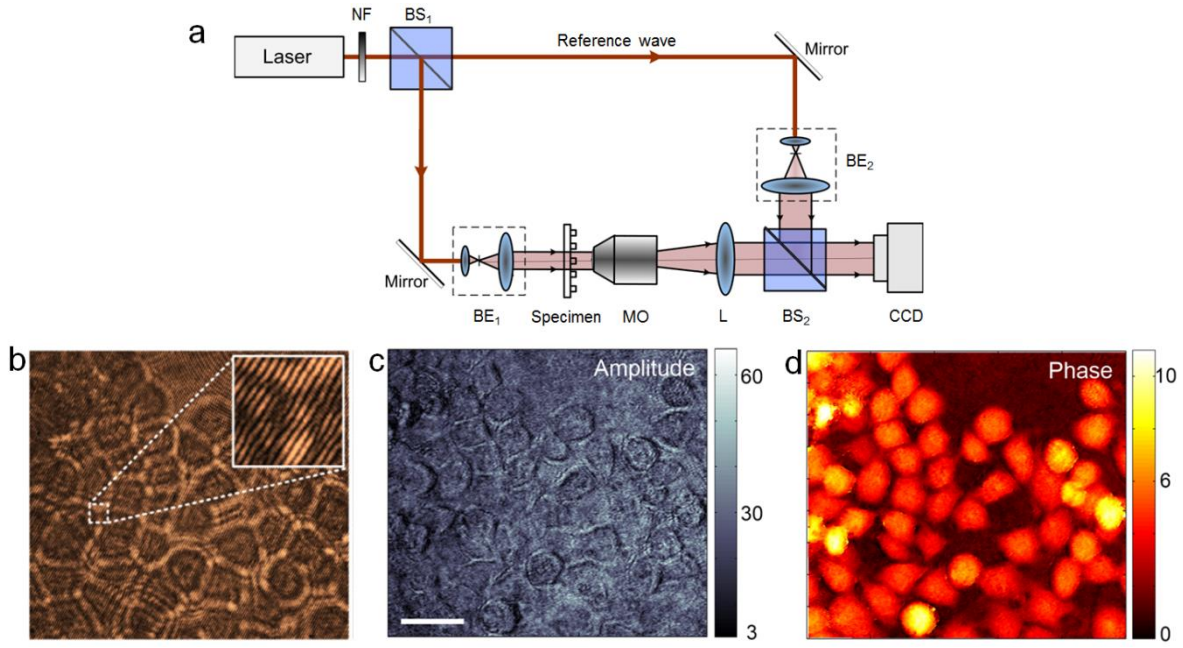

Figure 2. Basic configuration of DHM used with transparent or translucent specimens. (a) Schematic optical setup; (b) Recorded hologram example; (c) and (d) the reconstructed amplitude and phase images of the imaged sample. BE_1 and BE_2, beam expanders; BS_1 and BS_2, beam splitters; L, lens; MO, microscopic objective; NF, neutral variable attenuator. Scale bar in (c), 45 μm. Images taken from Ref. [21].

3.1 DHM with oblique illumination

In a regular DHM layout (Figure 2) where a microscope lens is used to image a specimen which is illuminated by a non-tilted plane wave, only the spatial-frequencies diffracted by the sample and up to a maximum value derived from the NA (~NA/λ) of the objective will be transmitted through the limited aperture of the microscope lens (Figure 3, upper part). The high spatial frequency content is diffracted at higher angles falling outside the limited lens aperture. However, when a plane but tilted wave is used as illumination (Figure 3, lower part), part of this higher spatial-frequency range is diffracted on-axis and, thus, will pass through the limited lens aperture. This downshift of the high spatial frequency range is recovered in a similar way than the centered spectrum aperture by DHM does. After multiplexing different incidence directions, a complementary set of apertures containing different spatial-frequency content is available and a synthetic aperture is generated as the coherent

Preprints (www.preprints.org) | NOT PEER-REVIEWED | Posted: 30 March 2018 doi:10.20944/preprints201803.0273.v1

addition of such aperture set. Figure 3 depicts the addition of 4 external apertures for synthetic aperture generation.

The reconstruction process is done digitally and the downshifted frequencies are back assembled to their original positions in the object's spectrum, thus synthesizing a wider spectrum than the one defined by the regular limited aperture. Final enhanced resolution image is achieved by inverse Fourier transform of the generated synthetic aperture. It is worthy to mention that the synthetic aperture synthesis is a coherent process where different phases need to be equalized and properly adjusted. These phase-mismatches come from different recording conditions of the different holograms, different aberrations terms per each tilted beam, and slightly mismatches in the experimental layout.

Using this strategy and despite that the spatial resolution of the regular imaging lens is modest, synthesized image can contain sub-resolution information. Here sub-resolution means that it contains details incoming from the spatial frequencies that are outside the conventional aperture under plane wave illumination. This is the reason why this type of techniques for resolution enhancenment are also named superresolution methods because it is related with the capability to overcome the resolution limit imposed by diffraction without changing the NA value of the lenses. So, given that the resolution limit in DHM under plane wave illumination is $0.82\,\lambda/NA$, it is improved to $0.82\lambda/[NA + sin(\alpha_{illum})]$ by using tilted beam illumination where α_{illum} is the tilted beam illumination angle.

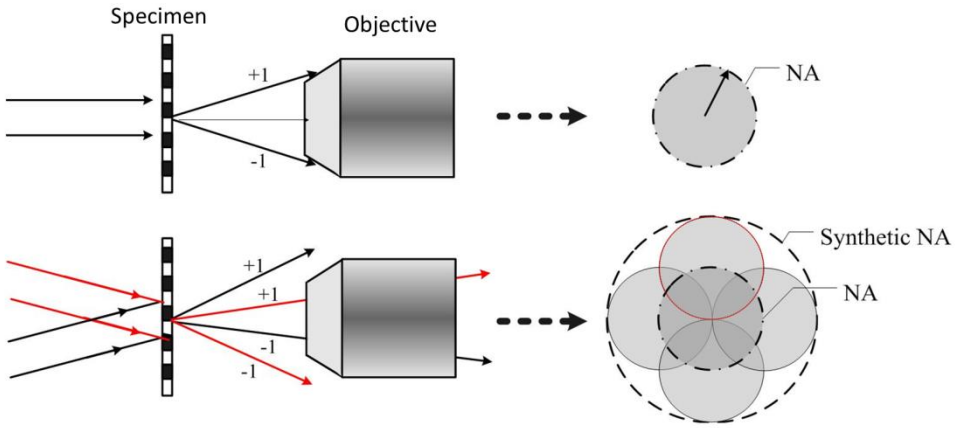

Figure 3. Schematics of oblique illumination and synthetic aperture generation.

Since the first implementations of superresolution by tilted beam illumination [85-88], many ways to synthesize a larger aperture via oblique illumination have been extensively reported in the literature [49,89-114]. Schwarz et al. used off-axis illumination to downshift the high-frequency components of the object's spectrum, and a reference beam is reinserted just at the proper angle to upshift the image content back to its proper spatial frequency region [65]. This process is performed twice for orthogonal illumination directions and sequentially in time, thus allowing the transmission of different frequency bands of the 2-D object's spectrum. The authors obtained a resolution gain factor of 3 for both orthogonal directions. Subsequent works demonstrate resolution improvement until the maximum limit for air-immersed optical imaging systems [90] as well as considering

 doi:10.20944/preprints201803.0273.v1

evanescent waves [102]. Also with optical rearrangement of the additionally transmitted spectral ranges, Mico et al. reported on the use of a vertical-cavity surface-emitting laser (VCSEL) array for resolution improvement [113]. In this case, the resolution improvement was 1-D but it was obtained with a single camera snap-shot with a resolution gain factor of 5. Extension to 2-D imaging was straightforward using different interferometric configurations [105,108-110] and synthetic numerical apertures above the maximum limit for air immersed imaging systems (NA = 1) was also reported [101]. Additional implementations considered wavelength multiplexing [95-97], and adaptation of tilted beam illumination techniques has been recently implemented into a regular upright Olympus microscope [92]. The use of scanning elements has also been reported as a technological improvement for providing tilted beam illumination [90,98,115,116], and sample rotation instead of tilt the illumination direction was also validated [74,100,102,107]. Tilted beam illumination for resolution enhancement has also been applied to differential interference contrast (DIC) microscopy [117] and Zernike phase contrast microscopy [118]. Moreover, axial rather than transversal resolution improvement has also been validated from the synthetic aperture generation [119] and an application of the technique to edge processing was also reported [120].

Just as an example of the results provided by the tilted beam illumination technique, Figure 4 shows the experimental results provided by the methods reported in Refs. [105,121] for different type of samples. Images in Figure 4(a,c) correspond to the central part of a high-resolution negative USAF test target, and (d-h) images are human red blood cells (RBCs). In the USAF case [105], a 0.14-NA, long working distance, infinity corrected microscope lens is synthetically expanded till approximately 0.45-NA. The generated synthetic aperture [Figure 4(b)] expands up by a factor of 3 the cut-off frequency of the regular lens (dashed white circle in Figure 4(b)) for every direction in the Fourier domain, thus allowing full 2-D resolution improvement. For the bio-sample, 2-D full space coverage of the sample's spectrum is again achieved (Figure 4(e)). A microscope objective with 0.1-NA is used to generate a synthetic aperture with an approximated value of 0.27-NA which enables RBCs visualization (Figure 4(f)) in comparison with the low-resolution images provided by the objective under conventional on-axis illumination (Figure 4(d)). Moreover, superresolved QPI is available since complex amplitude distribution is retrieved. This fact is demonstrated through Figures 4(g)-(f) where a 3-D view of the optical phase is represented.

Preprints (www.preprints.org) | NOT PEER-REVIEWED | Posted: 30 March 2018 doi:10.20944/preprints201803.0273.v1

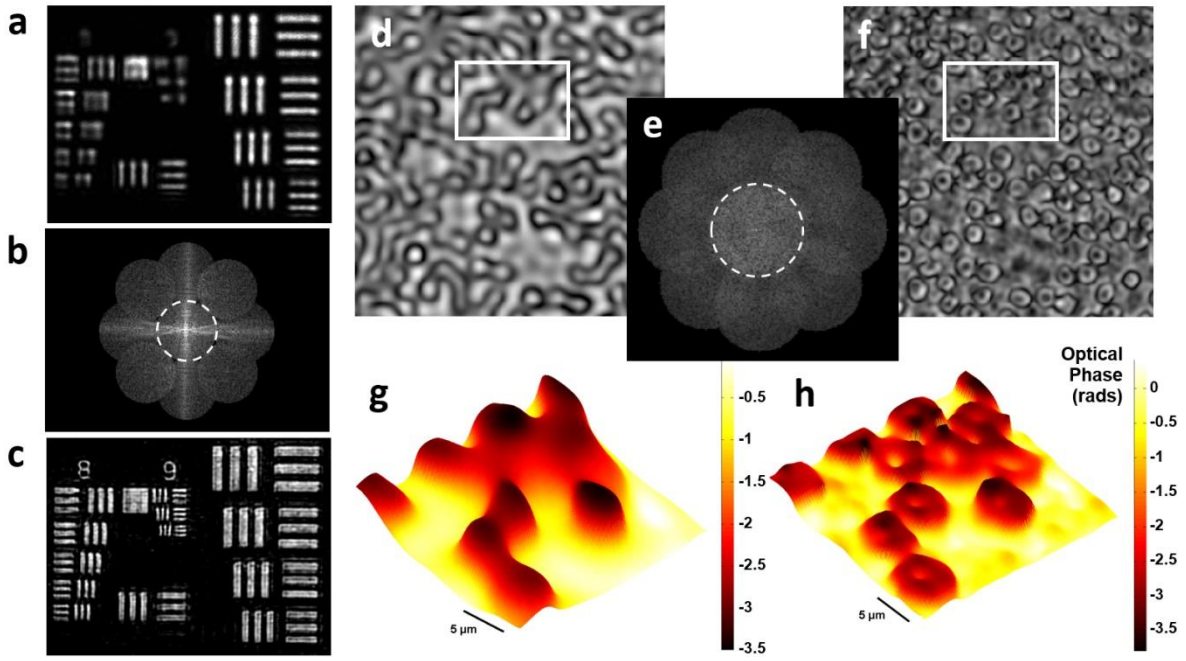

Figure 4. Demonstration of resolution-enhanced imaging using tilted beam illumination: (a-c) coming from Ref. [105] and (d-f) derived from Ref. [121].

3.3 DHM with structured illumination

Although structured illumination is typically used to obtain resolution improvement of intensity images [122,123], it has also been applied to resolution enhancement in DHM [66-71,124]. Figure 5(a) shows a setup used for the DHM with structured illumination [124], where the phase-shifting of the structured illumination was firstly implemented. In the implementation, four binary phase gratings rotated by m×45° (Figure 5(b)) and generated by a spatial light modulator (SLM) are projected onto the sample, so the sample is illuminated sequentially by 4 sinusoidal fringe patterns. After passing a telescope system comprised by the microscope objective *MO* and the lens *L*, the object wave interferes with a tilted reference wave *R* and the generated holograms are recorded by a CCD camera. We denote with Φ_{mn} the structured illumination wave generated by the grating having *m*th orientation and *n*th phase shifting, and with Ψ_{mn} the resultant wave transmitted through the object when becomes illuminated by Φ_{mn}. Thus, Ψ_{mn} interferes with the tilted reference wave *R* on the detector plane generating an intensity hologram in the form of $I_{mn} = |R + \Psi_{mn}|^2$. From this intensity, the wave Ψ_{mn} can be reconstructed by using standard methods as in off-axis DHM. Generally, Ψ_{mn} can be decomposed into three waves $A_{m,-1}$, $A_{m,0}$ and $A_{m,1}$ along the -1st, 0th and +1st diffraction orders of the illumination wave. When we assume that the phase increment for each shifting of the grating is α, then Ψ_{mn} can be written as:

$$\Psi_{mn} = \gamma_{-1}\exp(-in\alpha)A_{m,-1} + \gamma_0 A_{m,0} + \gamma_1 \exp(in\alpha)A_{m,1} \quad , \tag{1}$$

Preprints (www.preprints.org) | NOT PEER-REVIEWED | Posted: 30 March 2018 doi:10.20944/preprints201803.0273.v1

where γ_{-1}, γ_0 and γ_1 denote the magnitudes of the diffraction orders. From Equation (1) we can calculate the reconstructed object waves $A_{m,-1}$, $A_{m,0}$ and $A_{m,1}$ coming from the different diffraction orders and combined in the Fourier plane to yield the synthetic spectrum as:

$$\begin{bmatrix} A_{m,-1} \\ A_{m,0} \\ A_{m,1} \end{bmatrix} = \begin{bmatrix} \gamma_{-1}\exp(-i\alpha) & \gamma_0 & \gamma_1\exp(i\alpha) \\ \gamma_{-1}\exp(-i2\alpha) & \gamma_0 & \gamma_1\exp(i2\alpha) \\ \gamma_{-1}\exp(-i3\alpha) & \gamma_0 & \gamma_1\exp(i3\alpha) \end{bmatrix}^{-1} \cdot \begin{bmatrix} \Psi_{m1} \\ \Psi_{m2} \\ \Psi_{m3} \end{bmatrix} \quad (2)$$

Finally, a focused image with enhanced resolution is retrieved by inverse Fourier transform of the synthetic spectrum. As in previous tilted beam illumination approaches, the enhanced resolution limit in structured illumination DHM is determined by the illumination angle θ_{illum} of the +1 and -1 diffraction orders. Assuming the angular aperture of the imaging system (limited by the objective *MO*) is NA_{MO}, the synthetic *NA* of the structured illumination DHM is: $NA=NA_{MO}+\sin\theta_{illum}$ (Figure 5(c)). And this synthetic NA means an enhancement in spatial resolution, compared with the on-axis plane wave illumination where $\theta_{illum}=0$. Specifically, in the experiment [124], the NA_{MO} =0.25 of the objective lens limits the resolution of the set-up to δ_{plan}=1.55μm for the on-axis plane wave illumination. Using the structured illumination (with θ_{illum}=10 degrees), the resolution was improved to δ_{str}=0.9 μm. Particle-cluster on a glass plate (amplitude and phase object) have been used to validate the resolution enhancement of the described method (Figure 6). The phase images obtained by on-axis plane wave and structured illumination are shown in Figure 6(a,b), respectively. The phase image in Figure 6(b) has a better resolution compared with that in Figure 6(a) and two particles separated by 1.4 μm become distinguishable as shown in Fig. 6(c). The full width at half maximum (FWHM) of a single particle is 1 μm, which is slightly larger than the theoretical resolution value.

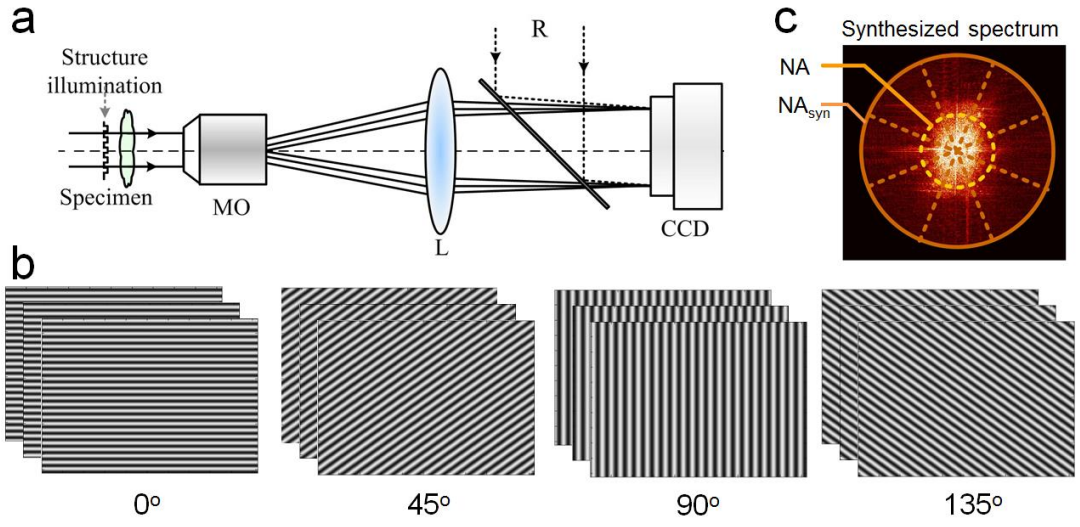

Figure 5. DHM with structured illumination. (a) Schematic setup; (b) four groups of structured illuminations with different directions; (c) the synthesized spectrum. Images taken from Ref. [124].

Structured illumination in DHM is completely analogous to the case of simultaneous illumination with two oblique plane waves at two different angles and provides the same effect

Preprints (www.preprints.org) | NOT PEER-REVIEWED | Posted: 30 March 2018 doi:10.20944/preprints201803.0273.v1

achieved by illuminating first at one angle and then at the other one. In fact, there is a complete parallelism between structured illumination and tilted beam illumination [85-121]. Although structured illumination leads to a larger amount of detectable sample frequencies than any single-beam illumination scheme, it does not contain more information beyond the diffraction limit [125]. Recently, structured illumination with unknown sinusoidal structured illumination has been exploited for DHM, for which an iterative reconstruction is needed to obtain resolution-enhanced images [69,126]. Structured illumination has also been applied in differential interference phase contrast (DIC) microscopy [127].

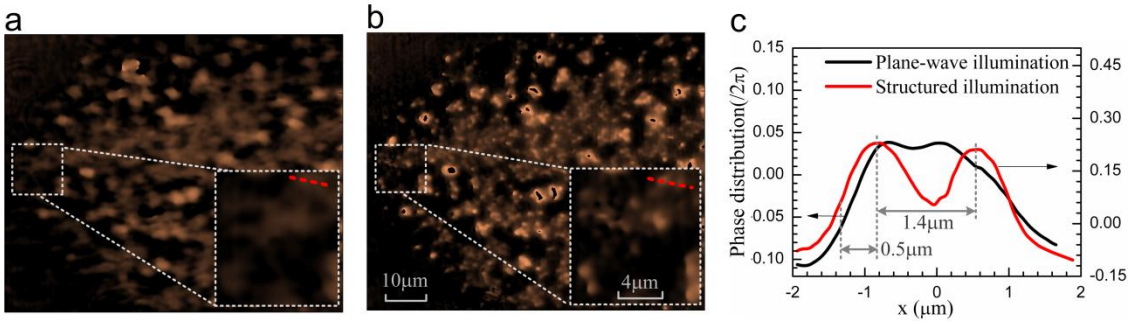

Figure 6. Experimental results for resolution enhancement in DHM with structured illumination. (a) and (b) reconstructed phase images by using plane wave illumination and structured illumination; (d) the phase distributions along the two lines drawn in (a) and (b). Images taken from Ref. [124].

3.4 DHM with speckle illumination

Speckle illumination can also be used to improve the spatial resolution of DHM. A speckle beam, which is generated by illuminating temporally coherent source through a diffuser such as a ground glass or a holographic diffuser, can be seen as a dozen of oblique illuminations with different angles. In incoherent microscopy, a dynamic diffuser changes the speckle patterns in time and, by utilizing full condenser aperture to improve spatial resolution and to reduce the effect of unwanted diffractions, it provides confocal-equivalent sectioning [128]. However, the phase information is lost during the time-averaging of the speckles. In order to retrieve phase information, each speckle field (including the information of both the targeted sample and the illumination pattern) should be recorded by interfering with a reference wave [128-130].

A typical setup of DHM with sequential speckle illumination [75] is shown in Figure 7. In the object wave path, a holographic diffuser (HD) is used to generate speckle field illumination. A galvanometric mirror (RM) before the HD controls the incident angle of the laser beam onto the diffuser and generates angle-dependent speckle fields. Two sets of angle-dependent speckle images were recorded, one with the sample and other without it. And two sets of object waves with and without the sample are reconstructed from the phase-shifted DHM holograms, which are obtained by utilizing the acoustic optic modulators AOM_1 and AOM_2. Then, a set of net angle-dependent electric-field images were obtained after dividing one set with the sample by the other without it and the sample-induced complex field image is retrieved. However, along with each speckle field, there are singular points (vortex) in the resulting amplitude and phase maps. To solve this problem, hundreds of speckle fields were recorded with and without the sample, and the reconstructed image

Preprints (www.preprints.org) | NOT PEER-REVIEWED | Posted: 30 March 2018 doi:10.20944/preprints201803.0273.v1

from these speckle illuminations were averaged to remove the speckle in reconstructed images. Compared to the phase images obtained with plane wave illumination (Figure 7(b,c)), the reconstructed images by using speckle illumination (Figure 7(d,e)) verify image resolution enhancement. Quantitatively, the full width half maximum (FWHM) of the point spread function was 516 nm for plane illumination and 305 nm for the speckle illumination, which are very close to the theoretical expectations.

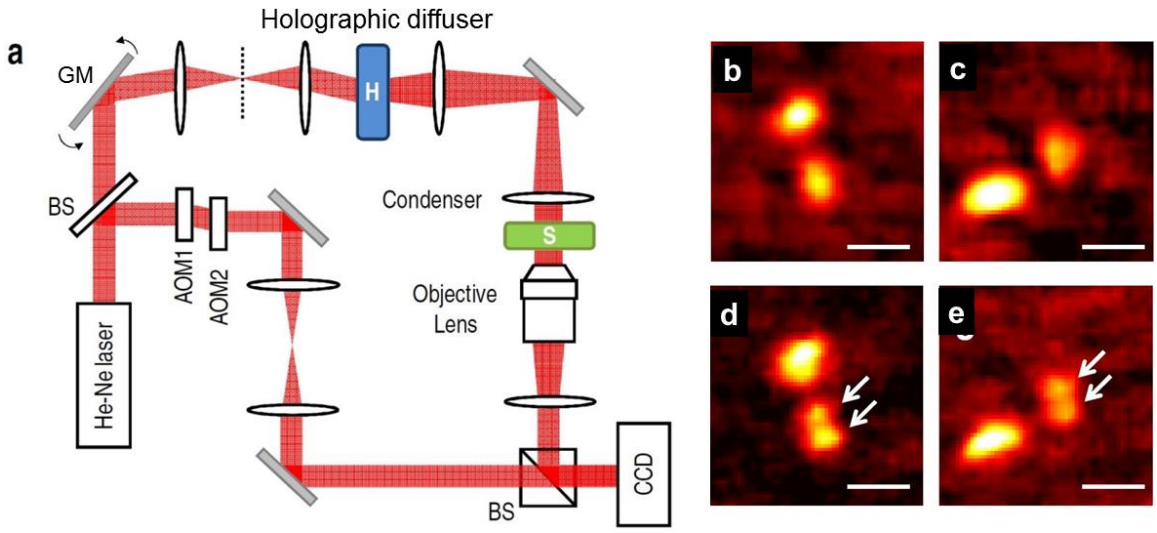

Figure 7. Schematics of DHM with sequential speckle illumination. (a) Experimental setup; (b)-(d) Phase maps of polystyrene beads (200nm diameter) under plane wave illumination (b-c) and speckle illumination(d-e). Scale bar in (d,e), 500 nm. Images taken from Ref. [76].

By using the aforementioned method, 3-D images of a sample with high spatial resolution, free of diffraction noise and with improved depth sectioning can be obtained. This method combines the advantages of incoherent imaging in resolution and image cleanness, with the merit of coherent imaging in complex electric-field recording and 3-D imaging. For the averaging operation, it is preferable to use a speckle field having the same weight or power along the whole frequency spectrum. Therefore, a highly-scattering device such as ground glasses or holographic diffusers are often used for speckle pattern generation.

Instead of this, an iterative reconstruction [80] was proposed. Figure 8 shows the optical setup used for that study and containing a spatial light modulator (SLM) for generating the speckle fields. The speckle fields illuminate the object after passing through the lens L_1 and the microscope objective MO_1. We denote with A_o^i the complex amplitudes of the fields diffracted by the object illuminated with the *i*th pattern. When no object is inserted in the setup the fields corresponding to the ith pattern are denoted with $A_{Speckle}^i$. Holograms are recorded by superimposing a reference beam R to the object $I_o^i = |A_o^i + R|^2$ and speckle fields $I_{Speckle}^i = |A_{Speckle}^i + R|^2$ from which A_o^i and $A_{Speckle}^i$ can be reconstructed.

Preprints (www.preprints.org) | NOT PEER-REVIEWED | Posted: 30 March 2018 doi:10.20944/preprints201803.0273.v1

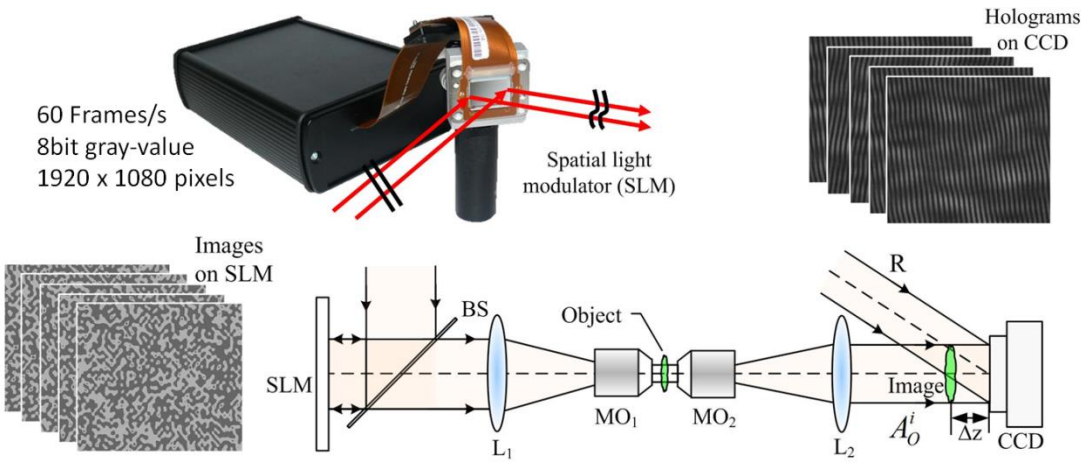

Figure 8. DHM with sequential speckle illumination. Images taken from Ref. [80].

As previously stated, speckle fields can be understood as a combination of plane waves with various illumination directions. Each one of those tilted illumination beams will shift the spectrum of the object in the reciprocal plane (see Figure 9(a)) allowing access to extra spatial frequencies. This extra information is integrated by an iterative method in order to synthesize the NA. The flowchart is shown in Figure 9(b) and essentially involves the following steps: 1) initialize the object wave $O(x,y)$ by averaging the complex amplitude of the reconstructed object wave $O_i = 1/N \cdot \sum_{i=1}^{N} A_o^i / A_{Speckle}^i$ for i =1 to N; 2) multiply $O(x,y)$ with the speckle illumination complex amplitude $A_{Speckle}^i$ to get the complex amplitude of the speckle-based object wave A_S^i; 3) perform the Fourier transform of A_S^i, and replace its central part (circle confined to a radius equal to NA/λ), with the corresponding part of the spectrum of A_o^i. The replacement operation bring new high frequencies which are downshifted by the speckle illumination $A_{Speckle}^i$; 4) determine the resolution-enhanced object wave $O(x,y)$ by taking the inverse Fourier transform, and dividing the retrieved complex wave A_{Syn}^i by $A_{Speckle}^i$; 5) continue the iteration by replacing the object wave $O(x,y)$ with the newly-reconstructed one. The iterative method enhances not only the resolution but also the signal to noise ratio (SNR) when the reconstructed object wavefronts from different speckle-based holograms are averaged. The use of an SLM for speckle field illumination avoids mechanical movements and allows high repeatability in comparison with dynamic devices.

Preprints (www.preprints.org) | NOT PEER-REVIEWED | Posted: 30 March 2018 doi:10.20944/preprints201803.0273.v1

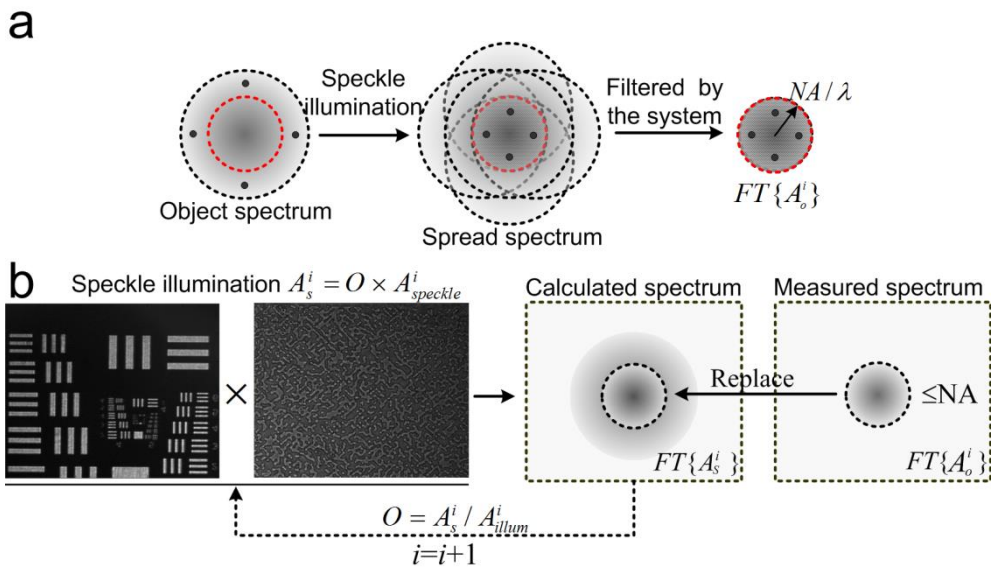

Figure 9. Iterative reconstruction of DHM with speckle illumination. (a) Frequency spectrum evolution in the imaging process; (b) iterative reconstruction with resolution enhancement. The red-dashed circles in (a) and the black-dashed circles in (b) represent the NA of the optical system. Images taken from Ref. [80].

3.5 *DHM with randomly-moving particles*

Another possibility for achieving resolution enhancement in DHM is by using particles in the close proximity of the specimen. This strategy can be subdivided into two main categories. In the first category, random movement of sparse particles is used for localizing with sub-resolution accuracy the transmittance change introduced by the sample's structure [131-134]. The superresolved image is retrieved after scanning the whole sample's area with the randomly-moving particles), and localizing their positions with a sub-resolution accuracy. In a few words, the random high-resolution pattern provided by the sub-resolution particles attached to the sample allows to shift the sub-resolution information in a similar way than tilted beam illumination produces. The constantly changing of the random distribution allows separation between the sub-resolution information and the original diffraction limited content. Thus, a proper resolving of the folded sub-resolution features is accomplished by multiplying each image in the stored sequence by the decoding pattern that is similar to the encoding one. The decoding pattern can be digitally extracted frame by frame from the set of low resolution recorded images since the particles are sparse. In any case, the particles should have a size below the resolution limit imposed by the imaging system. This type of methods can be seen as an evolution of the original idea reported by Françon in the middle of the past century [135] and based on synchronized moving pinholes, one over the object and another one at the image plane through an optical imaging system.

Figure 10 includes the experimental results reported using gold nano-particles (200 nm diameter) in Brownian motion for enhanced resolution imaging [133]. Figure 10(a) presents a SEM image of the resolution test target used in the experiment while Figure 10(b) shows the diffraction-limited image of the resolution-test target and corresponding with the conventional resolution image provided by the microscope lens (60X, 1.0-NA, water immersion, , Center Valley, PA, USA). The target is

Preprints (www.preprints.org) | NOT PEER-REVIEWED | Posted: 30 March 2018 doi:10.20944/preprints201803.0273.v1

illuminated with the white light source of a standard Olympus BX51 upright microscope, but a broad band interference filter (950 nm CWL, 50 nm FWHM, 25 mm Mounted Diameter, Edmund Optics, Tucson, AZ, USA) was previously inserted for experimental layout matching. According to the theoretical prediction, the resolution limit provided by the system is 475 nm, so the last resolved element is marked with a white rectangle at Figure 10(b) and corresponds to the bars having a pitch of 600 nm coming from a bar width of 350 nm and separated by a gap of 250 nm. Element S6 (with pitch equal to 471.3 nm) which is just in the limit of resolution but not resolved. Finally, Figure 10(c) depicts the superresolved image obtained by using the proposed approach. One may see that sub-resolution features corresponding with the elements labeled as S6-S5-S4, which cannot be seen in Figure 10(a), become now distinguishable in Figure 10(b). In order to further demonstrate the resolution improvement in the lower part of the Figure 10(a) as well as 10(b) we zoom in several demonstrative features of the obtained images. It is found that some bars of the superresolved image are resolved while the others are not (see for instance the vertical bars on Element S4). The reason is due to the random Brownian motion of the nanoparticles does not sweep enough such area.

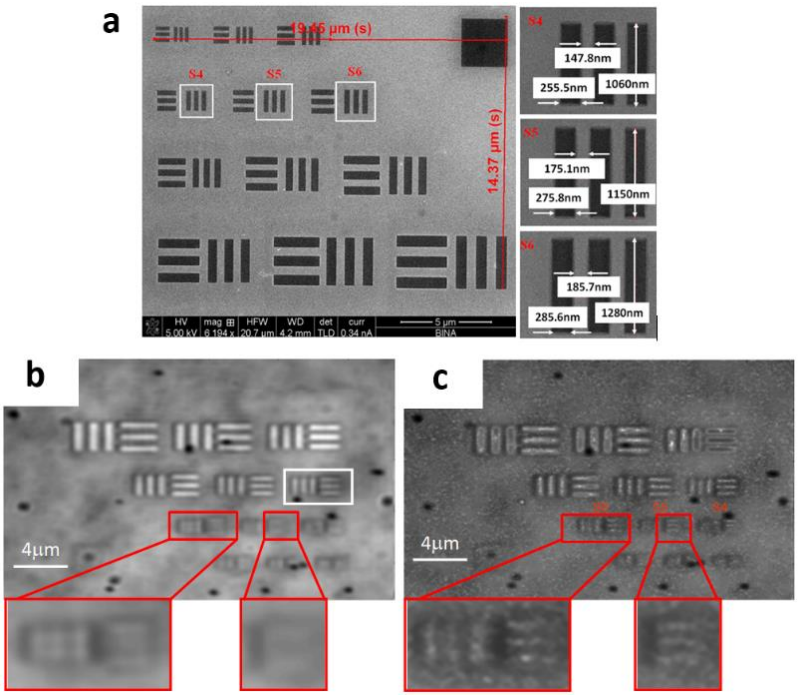

Figure 10. Resolution enhanced DHM with randomly-moving particles. (a) SEM image of the fabricated resolution-test target (left) and magnification of the elements S4-S5-S6 marked with a white square in the left image (right); (b) diffraction-limited image of the resolution-test target obtained when averaging the entire set of captured images; and (b) superresolved image containing sub-wavelength details. Images taken from Ref. [133].

As the second category, microsphere-based microscopy systems have garnered lots of recent interest mainly due to their capacity in focusing light and imaging beyond the diffraction limit [136,137]. The microspheres are placed on top of the sample and provide resolution enhancement by transforming the object wave from the higher frequencies to the lower ones. This new type of microscopy has been successfully applied to intensity-based microscopy [138,139] as well as to DHM

Preprints (www.preprints.org) | NOT PEER-REVIEWED | Posted: 30 March 2018 doi:10.20944/preprints201803.0273.v1

[140,141]. However, one of its main drawbacks is the very restricted FOV provided by the method since, essentially, the FOV is limited by the size of microsphere which is in the sub-wavelength range for having superresolution effect.

4. Resolution enhancement approaches in lensless DHM

Lensless holographic microscopy (LHM) is a relatively modern development raising from the same holographic principles as classical holography but using a solid-state image recording device (typically a CCD or CMOS camera) instead of the holographic plate recording media by. Nowadays, LHM is an emerging imaging modality with widespread interest where imaging is performed using a lensfree configuration. LHM derives from a digital implementation of the Gabor's invention [142] where a point source of coherent light illuminates the sample and the diffracted wavefront is recorded by a digital sensor [143].

LHM is typically implemented using two opposite layouts [144]. In the first layout, the sample is closely placed to the illumination point source and farther in comparison with the digital sensor [143,145-147]. And in the second layout, the illumination source is faraway while the sample is on top of the digital sensor [148-151]. The former configuration introduces a magnification factor (typically ranging from 5X to 20X) by geometrical projection of the sample's diffraction pattern at the digital sensor plane, and provides similar field of view (FOV) and resolution limit as reported in lens-based DHM with a medium NA (e.g., in the range of 0.4-0.5). The latter layout provides no geometric magnification (approximately 1X range) but an extremely improved FOV since the whole sensitive area of the detector is available. This second configuration provides a modest resolution limit incoming from lower NA values (0.2-0.3 NA range), mainly because of the geometrical constraints imposed by the detector. For the sake of simplicity, let us call the first implementation as digital in-line holographic microscopy (DIHM) while the second one will be referred as on-chip microscopy.

4.1 *DIHM with synthetic aperture*

In order to improve general capabilities (such as resolution in particular) of both previously commented configurations, many approaches have been reported mainly in the last decade. In the first case (sample magnified in the 5X-20X range), the resolution limit is ruled by diffraction in a similar way to that in DHM: there is an aperture in the system that limits the maximum range of spatial frequencies passing through the system. In LHM, the NA of the imaging system is defined by the ratio L/D with L and D being the half size of the digital sensor and the distance between the sample and the sensor. Thus, the resolution limit in DIHM can be improved scanning a larger hologram by applying different approaches. By scanning we mean a relative motion between the object and the digital camera and it implies the generation of an expanded hologram containing a bigger portion of the diffracted object wavefront compared to the non-scanning case.

The generation of the expanded hologram can be implemented using, in essence, 4 different strategies. The first strategy (and maybe the most appealing one) deals with the displacement of the camera at the recording plane [152-164] thus synthesizing a larger hologram in comparison with that one provided by only one camera position. The second strategy performs synthetic aperture generation by angular multiplexing the spectral object information [97,165-172]. Angular multiplexing is implemented by tilted beam illumination over the object in a similar way as in DHM and allows the recovery of additional spatial frequencies falling outside the digital camera sensible

 doi:10.20944/preprints201803.0273.v1

area when on-axis illumination is used. The third strategy is related with the use of additional optical elements (typically diffraction gratings) that are placed between the object and the digital camera [76,173-179]. The diffraction grating directs towards the camera an additional portion of the diffracted object wavefront allowing the generation of the synthetic aperture hologram. And finally, the fourth strategy is based on object movement instead of shifting the digital camera for aperture synthesis [180-183].

As one can notice, the four strategies are equivalent and the effective outcome of each one of the four encoding strategies is the same one: to downshift extra content of the object spectrum that usually falls outside the limited system aperture with conventional illumination. This downshift allows the recovery of such extra apertures using different decoding methods and depending on the used encoding one. Figure 11 includes 4 cases of experimental results regarding synthetic synthesis in DIHM when considering the 4 previously reported strategies. By rows and from up to down, Figure 11 includes (a) camera shifting, (b) tilted beam illumination, (c) diffraction grating insertion and (d) object scanning for superresolution in DIHM. And by columns and from left to right, Figure 11 presents the conventional low-resolution image (left), the generated synthetic aperture (center) coming from the addition of elementary apertures (white dashed rectangles) in comparison with the conventional aperture (central blue solid line rectangle), and the superresolved image as inverse Fourier transform of the synthetic aperture (right). Notice that in DIHM the conventional aperture shape is rectangular rather than circular as in DHM since it is the CCD the element defining the system's aperture.

Preprints (www.preprints.org) | NOT PEER-REVIEWED | Posted: 30 March 2018 doi:10.20944/preprints201803.0273.v1

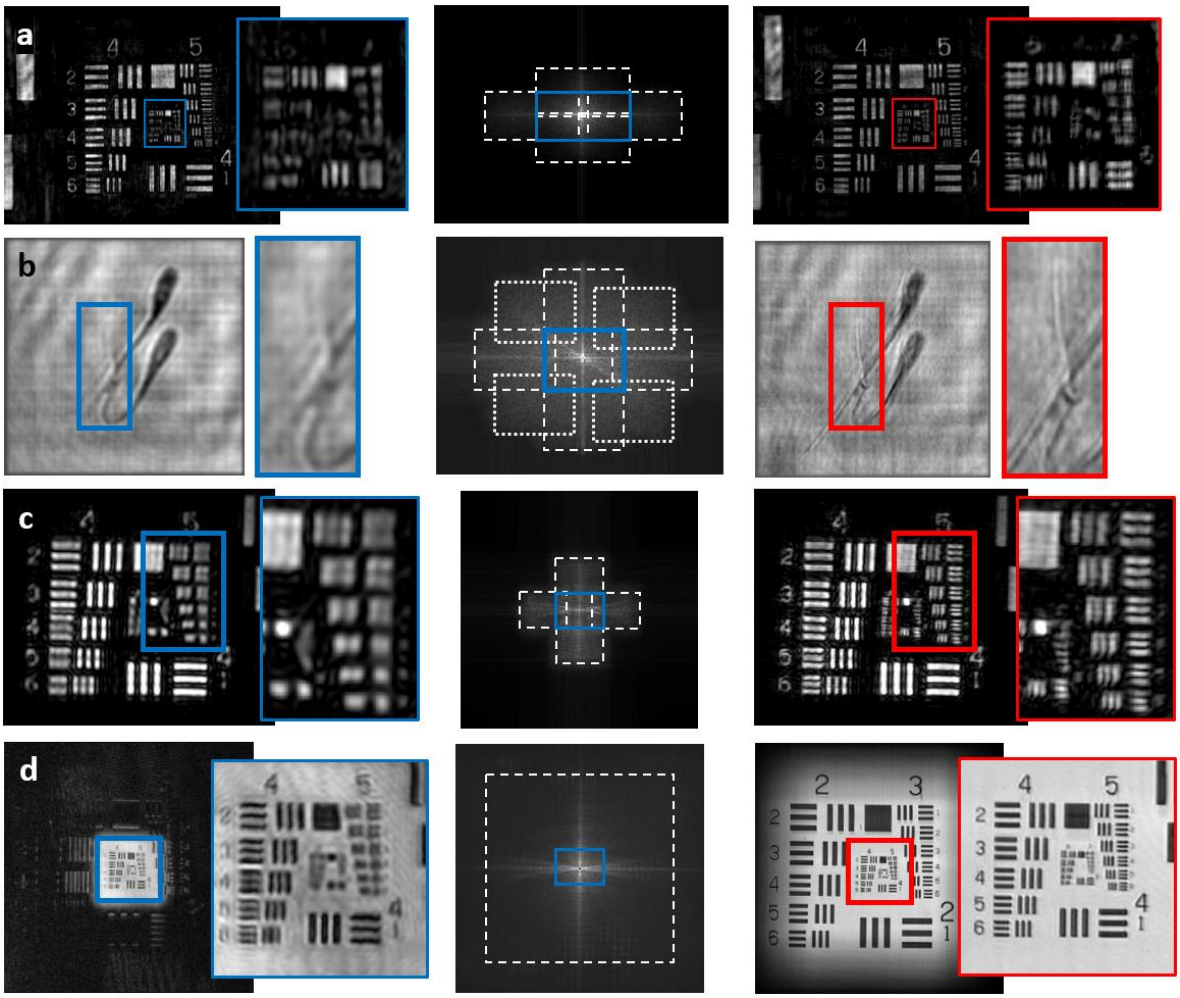

Figure 11. Experimental results for resolution enhancement of DIHM via (a) shifting the camera at the recording plane (first row – images taken from Ref. [159]), (b) using tilted beam illumination (second row – images taken from Ref. [169]), (c) inserting a grating in the experimental layout (third row – images taken from Ref. [176]), and (d) considering object movement at the input plane (fourth row – images taken from Ref. [181]). Inside each column, the conventional image without aperture synthesis (left images), the generated synthetic aperture (central images), and the finally retrieved superresolved image (right images). In each row, the central parts was magnified to allow easy identification of the superresolution effect.

The first row of Figure 11 shows the experimental results obtained by shifting the camera [159] doubling the resolution of the conventional imaging system. The camera was shifted at the image plane in the horizontal and vertical directions since most relevant information of the object is in those directions. But the synthetic aperture shape can be customized according to such a priori object information. As an example, a cross-shape synthetic aperture (central image) was generated with expanded frequency coverage that finally yields in an isotropic resolution-enhanced image (right image) in comparison with the conventional one (left image). The resolution limit is expanded from 12.4 μm (Group 6-Element 2 of the USAF test) until 6.9 μm (Group 7-Element 2) for the horizontal CCD direction, revealing a resolution gain factor close to 2.

Tilted beam illumination downshifts the spatial frequency information of the object so the synthetic enlargement of the system's aperture can be achieved without camera displacements. Here,

 doi:10.20944/preprints201803.0273.v1

an illumination pinhole is shifted to different off-axis positions in order to provide tilted beam illumination. To allow this, the sample should be static between the different recordings, so the technique is using time multiplexing for aperture synthesis. Figure 11 (second row) includes the experimental results reported in Ref. [169] and concerning a fixed swine sperm bio-sample. In this case, the 4 apertures in the vertical and horizontal directions and the 4 apertures in the oblique directions were considered. As a consequence, full 2-D coverage at the Fourier domain is achieved when generating the synthetic aperture. Using this strategy, a synthetic numerical aperture close to 0.7 was experimentally validated for the largest CCD direction.

Figure 11 (the third row) depicts the experimental results concerning enhanced resolution imaging by properly inserting a diffraction grating in the lensless Fourier holographic experimental layout [176]. Depending on the Fourier spectrum of the diffraction grating, the superresolution effect can be 1-D or 2-D. Two possibilities can also be considered for retrieving the complex amplitude distribution of each band-pass image depending on the mode that the reference beam is introduced in the recording plane: on-axis recording with phase shifting algorithm and off-axis recording with Fourier domain filtering. Thus, it is possible to choose between a superresolved image over a large object FOV or a higher number of band-pass by limiting/masking the object´s FOV. Here, a cross-shape synthetic aperture is generated yielding in a resolution gain factor of 2 in both directions. According to the images included at Figure 11, the resolution limit is improved from 31.25 μm (Group 5-Element 1 of the USAF test) until 15.6 μm (Group 6-Element 1) for the horizontal CCD direction.

Last but not the least, aperture synthesis has also been reported by using the object translation as key tool for image quality improvement in LHM [181,182]. Lensless Object Scanning Holography (LOSH), profits of the linear movement of the object to record a set of reflective digital lensless Fourier holograms. Because of the linear object displacement, different spatial information coming from different object's regions of interest (ROIs) is recorded in each hologram and retrieved later on. Meanwhile, each single ROI passes along the whole FOV in front of the CCD and becomes illuminated with a different tilted beam for every position, thus allowing for retrieve different spatial frequency content of every ROI. Those two characteristics produce object FOV enlargement and resolution improvement, respectively, when considering the whole set of recorded holograms. Moreover, the SNR of the final image is also enhanced due to the averaging of the coherent noise when adding the whole set of recorded holograms. As a result, the final image provided by LOSH resembles an image obtained under white light illumination but considering that not only intensity but also phase information is accessible. Thus, an extended DOF image can be also synthesized owing to the coherent nature of LOSH by numerical propagation to different axial distances. Figure 11 (last row) shows the experimental results provided by LOSH where an impressive image quality improvement concerning FOV, resolution and SNR is achieved for a 2-D resolution test. The scanning was performed using a regular raster composed by 20 rows and 20 holograms per each row. As a consequence, the conventional FOV (1.5x1.5 mm, approx.) is expanded up to a synthetic FOV 3.7 time higher (5.5x5.5 mm, approx.), the resolution limit is enhanced from 44 μm to 14 μm meaning a resolution gain factor equal to 3.2, approx., and the SNR value is improved from 2.34 (single hologram) to 10.16 (superresolved image) after applying LOSH yielding in a SNR gain factor of 4.34.

4.2 *On-chip microscopy with geometrical superresolution*

Preprints (www.preprints.org) | NOT PEER-REVIEWED | Posted: 30 March 2018 doi:10.20944/preprints201803.0273.v1

Coming back to our two opposed layouts in LHM, resolution enhancement methods have also been reported using on-chip microscopy (1X sample's magnification). In the on-chip microscopy, sample are placed really close to, or, directly contact with the imaging sensor, so the limiting factor in resolution is essentially the pixel size of the digital sensor that defines the sampling requirements and the coherence properties of the illumination source which defines the maximum angle that a diffracted beam will interfere with the non-diffracted reference beam. In this configuration, an immersion medium with the refractive index higher than 1 fills the gap between the sample and the sensor since there is glass coming from the coverslips containing the sample. Such immersion scheme enhances the resolution in comparison with the previous DIHM layout where air is filling the gap.

Nowadays, there are available sensors having a pixel size at the micron range yielding resolution limits that are similar to that of the DHM systems having microscope lenses with 0.25-NA for a visible illumination. Despite the spatial resolution can be improved by reducing the pixel dimensions, doing this the signal-to-noise ratio (SNR) will be reduced. To circumvent this conflict between the resolution and the SNR, pixel superresolution (or geometrical superresolution) was proposed and successfully applied to on-chip microscopy [144,184-197]. This strategy recods sequentially multiple images of the same sample when the sample is shifted along the horizontal and vertical directions for a sub-pixel distance each time. These sub-pixel shifts synthetically reduce the effective pixel size of the camera, so the final resulting image exhibits a higher resolution limit from a sampling point of view.

Similar to the previous DIHM configuration, the shift is relative between the sample and the digital recording device. So, it is possible to shift the digital sensor [196,197], the sample [194,195], or the illumination [190-193] but keeping static the rest of the setup. However, the most practical technique is to shift the illumination source because precise subpixel shifts can be generated from less-precise illumination shifts due to the geometrical characteristics of the layout (distance's ratio between the illumination-to-sample and the sample-to-digital sensor). Nevertheless, other approaches have been reported using wavelength scanning [188,189] or multiple intensity images at different sample's distances [186,187]. Using these types of approaches, resolution limit in LHM has approached diffraction limited resolution limit with half-pitch resolutions equivalent to those from 0.8-0.9 NA microscope lenses [144, 190].

Finally, similar to the previous DIHM configuration, synthetic aperture generation has also been proposed as a way to increase the resolution limit in on-chip microscopy [184]. Here, the illumination source is not only shifted to achieve geometrical superresolution by subpixel shifts but tilted to allow oblique illumination and aperture synthesis. Thus, a set of multiple low-resolution holograms (typically between 16 and 64) for each tilted beam illumination position (11 oblique illuminations for each orthogonal direction) are recorded and then used to achieve geometrical as well as diffraction limited superresolution imaging. By digitally combining all those lensfree holographic measurements, the authors clearly resolved 250-nm grating lines under 700-nm illumination wavelength which effectively corresponds to a 1.4-NA.

In addition to those holographic approaches, on-chip microscopy with enhanced resolution has also been applied to other imaging modalities such as fluorescent imaging [198-201], structured illumination [198], holographic color imaging [188,191,202] and as specific arrangement for cell culture [203,204] and waterbone parasites analysis [150] in combination with deep learning

Preprints (www.preprints.org) | NOT PEER-REVIEWED | Posted: 30 March 2018 doi:10.20944/preprints201803.0273.v1

microscopy [205,206] as well as 3-D tracking of sperm cells trajectories [207-209] based on improved axial resolution [210].

5. Resolution Enhancement of Reference-less QPM

Phase imaging based on interferometric methods is the most commonly used approach to retrieve phase information. It presents high accuracy, but sometimes the need to introduce an additional reference wave improves its complexity. Moreover, the measurements are sensitive to environmental disturbances coming from thermal and/or vibration conditions that are different on both interferometric beams. To circumvente this difficulty, reference-less phase imaging approaches have been exploited in both DHM and LHM.

Regarding DHM, a wide range of techniques have been developed in the last years for achieving QPM without interferometric tools. This category includes, just to cite a few, wavefront sensing based on Shack–Hartmann sensors [7,211,212], pyramid sensors [8,213], or shearing systems [214,215]. Other approaches are based on common-path interferometric configurations and are capable of reference beam synthesis from the object beam in order to avoid the external reinsertion of a reference beam [216-218]. Others utilize a TIE algorithm with slightly defocused images for QPI [219-223] while others are based on the recording of different defocused images of the sample to iteratively retrieve phase information [224,225]. Alternatively and in LHM, beam-propagation-based methods can also retrieve quantitative phase information from the recording of a series of diffraction patterns, which are usually recorded at different planes [28,29], with different wavelengths [33-36,226], by moving sub-apertures over the sample plane [30], by modulating the object wave with different phase patterns [31], or by using modulated illuminations [32].

5.1 Reference-less phase retrieval with modulated illumination

Here we depict the first type of single-beam QPM with resolution enhancement by using modulated illumination [32,227]. Figure 12(a) shows the setup used for sQPM which is similar to the one used in Section 3.4 but no reference wave is needed. The random patterns on SLM (insets in Figure 12(a)) are projected to the sample plane by the relaying system (L_1-MO_1). After passing through the sample placed in the focal plane of MO_2, the object wave is imaged by the system MO_2-L_2 and the diffraction pattern (Figure 12(a), inset) are recorded by a CCD camera located at a distance Δz from the image plane IP of the specimen.

Because these random phase patterns are generated using an SLM, they are highly repeatable and their complex amplitudes can be measured in advance. We denoted them with A_{illum}^{k}, and k=1,2,…M while I^k denotes the diffraction pattern of the object wave under A_{illum}^{k}. The phase retrieval is performed using the following steps: (1) multiply the amplitude of the k^{th} diffraction pattern with a random initial phase factor exp ($i\varphi^k$); (2) propagate $\sqrt{I^k}\exp(i\varphi^k)$ to the object plane; (3) the calculated wave is divided by the k^{th} illumination amplitude A_{illum}^{k}, and multiplied by the $(k+1)^{th}$ illumination amplitude A_{illum}^{k+1}; (4) propagate the newly-obtained object wave to the CCD plane; (5) replace the amplitude of the obtained object wave with $\sqrt{I^{k+1}}$; (6) repeat the iteration loop (2)–(5) by using k+*1* instead of *k*, until the difference between two neighboring reconstructions will be smaller than a

Preprints (www.preprints.org) | NOT PEER-REVIEWED | Posted: 30 March 2018 doi:10.20944/preprints201803.0273.v1

threshold value. Furthermore, the object waves reconstructed from different groups of those random-phase illuminations are averaged in order to reduce the noise. Figure 12(b) shows a representative phase image obtained by using sQPI. Notably, the spatially modulated illumination also improves the spatial resolution of the phase imaging since it scrambles the specimen spectrum and, thus, some high-frequency components of the object wave beyond the NA of the system are downshifted and can pass through the limited system aperture. These high-frequency components are shifted back to their original positions during the iterative process and the resolution of the imaging becomes improved. Figure 12(c) shows the resolution enhancement of sQPM, compared with the DHM with plane wave illumination.

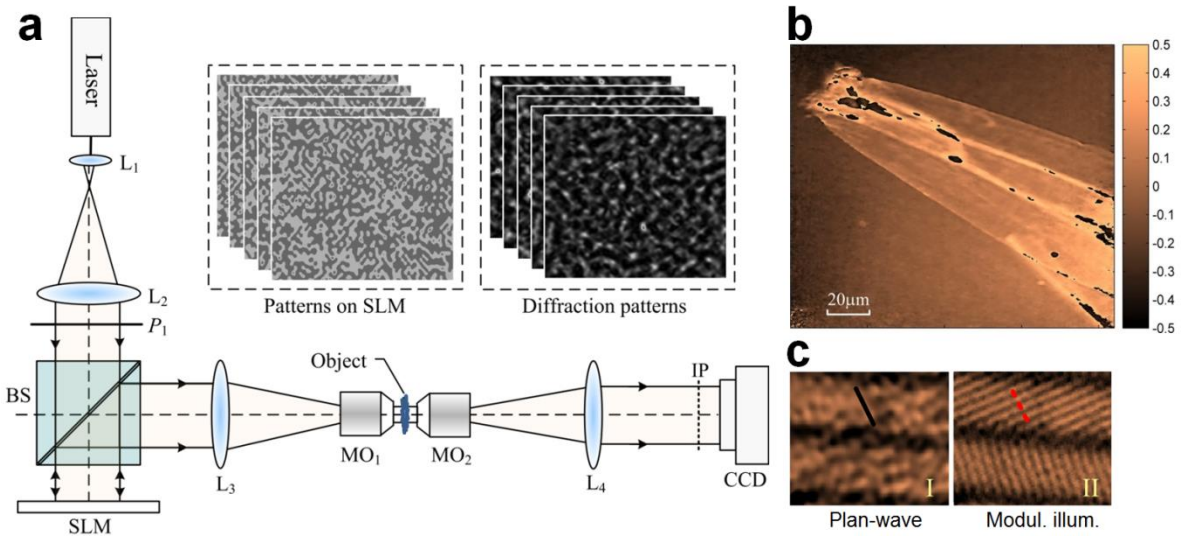

Figure 12. Single-beam QPM using modulated illumination. (a) schematic setup; insets in (a) show the phase patterns displayed on SLM (left) and the diffraction patterns recorded by the CCD camera (right); (b) Representative phase image obtained by using sQPM; (c) resolution comparison of DHM with plane wave illumination (I) and sQPI with modulated illumination (II). Images taken from Refs. [32,227].

5.2 Reference-less QPI with aperture synthesis

Another interesting approach for superresolution in reference-less QPI comes from the combination of tilted beam illumination and phase retieval using an iterative algorithm [115,228]. The basic idea of the iterative algorithm is to record a sequence of defocused intensity images at N planes and then process these images to extract the phase encoded in the defocus. The different intensity planes are generated by linear translation of the camera [229] or without moving parts using a tunable lens [228]. The procedure is quite similar to the previous references [224,229] but now tilted beam illumination is considered aside of the on-axis conventional illumination. Thus, the phases at multiple illumination angles are retrieved and a synthetic aperture can be generated as the coherent addition of the retrieved information coming from different shifted pupils. The main drawbacks of the method are: i) the sequential recording of the different N intensity images that prevents the use of the technique for fast dynamic samples; ii) the need for mechanical scanning of both the tilted beam illuminations (using galvo mirrors) and the camera shift (linear motorized translation stage); and iii) the inherent

 doi:10.20944/preprints201803.0273.v1

limitation of the method to transmit the background beam at oblique illuminations for phase retrieval meaing that the maximum resolution gain factor is intrinsically limitted to a factor of 2 (authors demonstrated a resolution gain factor equal to 1.3). We note that the resolution enhancement approaches of the on-chip microscopy also belongs to this category.

As we have previously stated, another completely different possibility for QPI in reference-less approaches is to perform reference beam synthesis from the diffracted object wavefront [219-225,230]. Alternatively, the point-diffraction phase microscopy [23,26] generates a reference beam by pinhole-filtering on one copy of the object wave. The setup has the advantages of being less sensitive to environmen-tal vibration and high lateral and phase resolution. In that sense, SMIM (initials incoming from Spatially-Multiplexed Interferometric Microscopy) proposes a simple and low-cost way to convert a commercially available regular microscope into a holographic one with only minimal modifications [231,232]. SMIM implements a common-path interferometric setup into a real microscope embodiment where: i) the broadband light source is replaced by a coherent one; ii) a 1-D diffraction grating is properly inserted at the microscope embodiment; and iii) a clear region at the input plane is saved for reference beam transmission. Using SMIM, a regular microscope is converted into a holographic one working under off-axis holographic recording with Fourier filtering [231] or slightly off-axis recording with phase-shifting algorithm [232]. The apealling advantage above the convetional DHM is the stability (less sensitive to environmental disturbance) due to the common-path configuration.

Maybe the main drawback of SMIM is the FOV restriction imposed by the need to transmit a clear transparent reference beam for the holographic recording. Despite the FOV is penalized,the resolution will be improved in SMIMwithout modifying a given optical imaging configuration. In order to improve the resolution of SMIM, tilted beam illumination has been recently adapted to the SMIM architecture [92]. Tilted beam illumination is achieved by lateral displacement of the coherent source to a set of off-axis positions, thus allowing a complementary spatial-frequency content diffracted on-axis for each considered tilted beam (a regular procedure in oblique illumination techniques). And SMIM technique recovers the complementary spatial-frequency content provided by each tilted illumination. In addition to the on-axis one, the full set of tilted beam illuminations are used to expand up the system's aperture by generating a syntehtic aperture having a cutoff frequency two times higher than that of the conventional one under on-axis illumination. All together, suprresolved SMIM adapts a commercially available non-holographic microscope into a superresolved holographic one. When applying SMIM with the 5X/0.15NA lens, the resolution is doubled and the useful FOV of is reduced to one half [232]. The FOV is still equal to the one provided by the 10X/0.30NA lens which is often employed to reach the same resolution with suoperresolved SMIM. Figure 13 depicts the experimental results provided by this method [92] when using a 5X/0.15NA objective lens. The conventional image (left) corresponding with on-axis illumination mode is restricted in resolution and comes from the inverse Fourier transform of the conventional pupil (blue circle in the central image). Then, tilted beam illumination procedure is implemented allowing the recovery of 4 extra off-axis apertures that are used to synthesize the expanded aperture (center). Finally, the superresolved image (right) showing a resolution enhancement by a factor of 2 is achieved from the syntetic aperture.

Preprints (www.preprints.org) | NOT PEER-REVIEWED | Posted: 30 March 2018 doi:10.20944/preprints201803.0273.v1

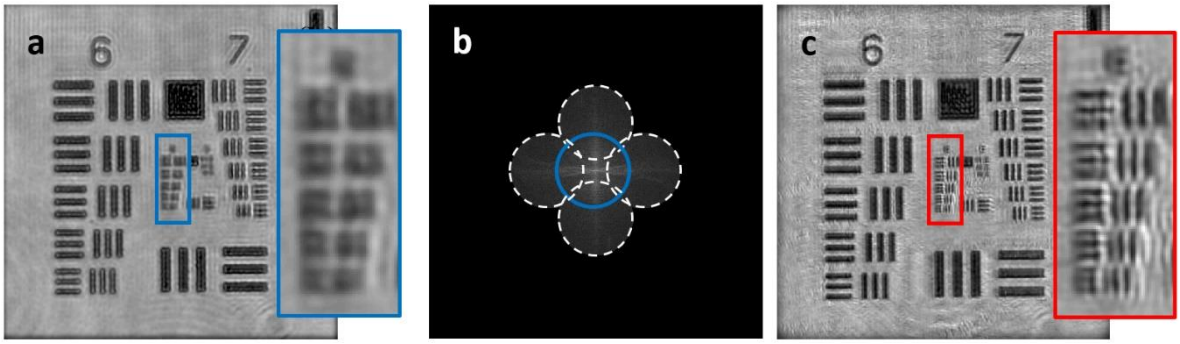

Figure 13. Experimental results for superresolved imaging of SMIM using tilted beam illumination. The low-resolution image retrieved with on-axis illumination (a), the generated synthetic aperture (b), and the finally retrieved superresolved image (c). Images taken from Ref. [92].

5.2 Fourier ptychographic microscopy (FPM)

Another reference-lens QPM approach with resolution enhancement capability is termed with Fourier ptychographic microscopy (FPM) [39,233-237]. This method uses successive illuminations at different directions to recover a high-resolution and high-SBP output image by iteratively stitching together a number of low-resolution images in Fourier space.

In FPM, a sample is placed at the focal plane of a microscope objective often with a low-NA (Figure 14). The light from different LEDs in a source-coded LED array is used to illuminate the sample at different directions/orientations. A sequence of images is collected with the sample successively illuminated by plane waves at different propagation angles from different LEDs. Then, an iterative process is used to reconstruct a high-resolution image from the recorded low-resolution images. (1), initialize the high-resolution image, $\sqrt{I_h}e^{i\varphi_h}$ with φ_h=0 and I_h as any upsampled low-resolution image as a starting point. (2) generate a low-resolution image $\sqrt{I_1}e^{i\varphi_1}$ by selecting a circular region on the spectrum of $\sqrt{I_h}e^{i\varphi_h}$ and taking inverse Fourier transform. The position of the circular region corresponds to a particular angle of illumination, and the size of the region given by the coherent transfer function of the objective lens. (3) replace I_1 by the measured intenisty I_{1m}, and update the corresponding region of $\sqrt{I_h}e^{i\varphi_h}$ in Fourier space. Here the subscript m indicates the m^{th} measured intensity. (4) repeat steps (2)-(3) for other plane-wave incidences (total of N intensity images). (5) repeat steps (2)-(4) till a self-consistent solution is achieved. Eventually, the converged solution in Fourier space is transformed to the spatial domain to recover a high-resolution image of the targeted sample with a dramatically increased SBP (namely, high-resolution and wide-FOV).

However, the increase of SBP is paid with long acquisition time, typically in the order of minutes. Faster capture times, once achieved, will improve the imaging speed and consequently, allows studying live samples, which is continuously evolving at various spatial and temporal scales [237]. And scheems exhibiting the working principle of high-speed aperture synthesis are also recently reported [238,239]. A smart implementation scheme on source-coded LED array, together with an improved algorithm, was proposed to increase the speed of FPM with enhanced SBP. In order to further improve the resolution enhancement range, an oil-immersion condenser was employed to enlarge the illumination angle [240]. Furthermore, instead of enlarging NA_{ill}, FPM is also implemented by using a high-NA imaging objective, proving a final NA_{syn} of 1.4536 [235].

Preprints (www.preprints.org) | NOT PEER-REVIEWED | Posted: 30 March 2018 doi:10.20944/preprints201803.0273.v1

Besides the aforesaid two types of resolution-enhanced single-beam QPM, annular illumination was used to improve the spatial resolution of on Zernike phase contrast [118] or transport-of-intensity equation (TIE) [241] based QPM. In addition, LED array was also used in differential phase contrast microscopy [242].

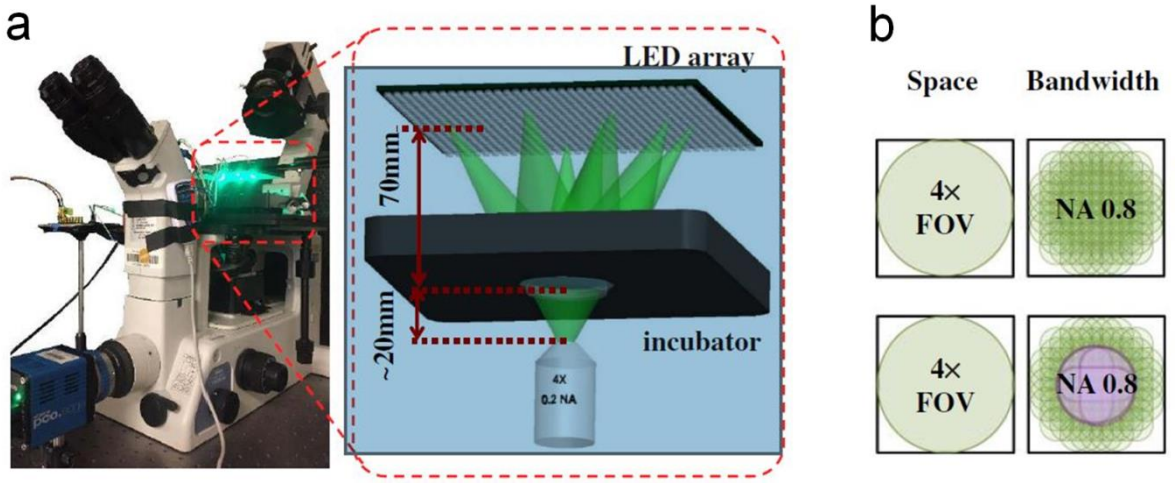

Figure 14. Schematics of Fourier ptychographic microscopy (FPM, modified from the reference [238]); (a) experimental setup of FPM with a source-coded LED array; (b) bandwidth extension of FPM. Images taken from Ref. [238].

6. The criterion for evaluating the resolution of QPM

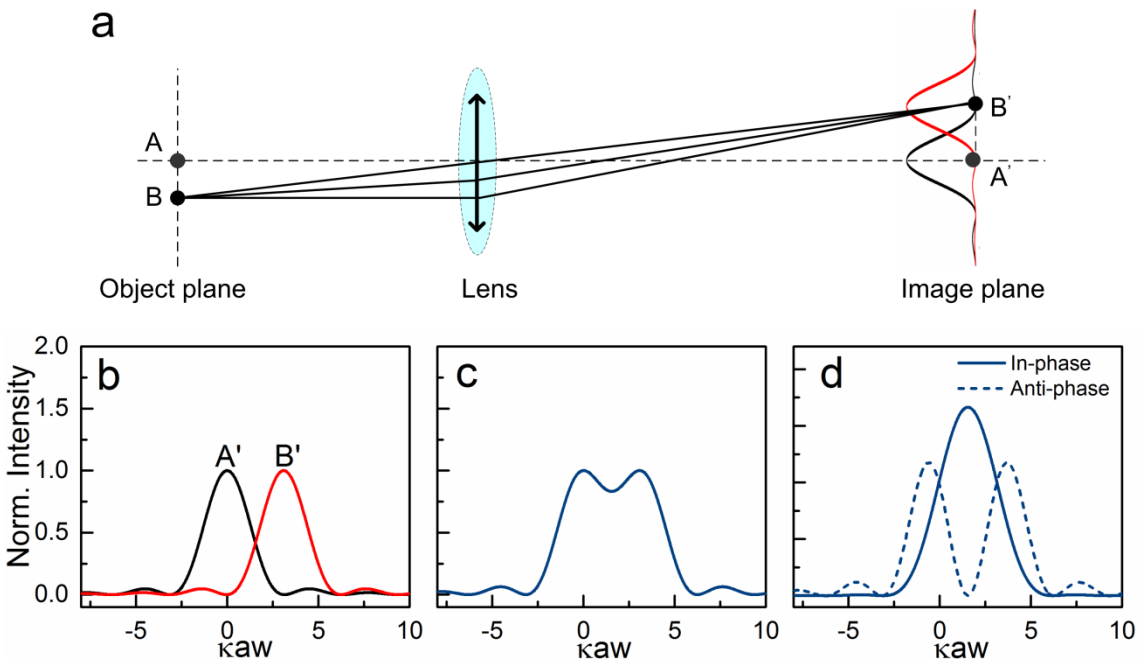

Figure 15. Comparison of the resolution of incoherent and coherent microscopy. (a) Schematics illustrating the resolving power of a microscope; (b) intensity distribution of the Airy patterns A′ and B′ obtained by imaging two infinitely-small point sources A and B through a diffraction-limited system; superimposed intensity of A′ and B′ in the case of incoherent (c) and coherent microscopy

Preprints (www.preprints.org) | NOT PEER-REVIEWED | Posted: 30 March 2018 doi:10.20944/preprints201803.0273.v1

(d). "In-phase" and "Anti-phase" in (d) indicates the case A and B have the phase difference 0 and p, respectively.

Here we first examine the resolving power of incoherent microscopy and coherent microscopy with two neighboring points (with infinitely small diameter), separated by a distance w_1 in the object plane (Figure 15(a)). The imaging system of an incoherent or coherent system produces in the image plane two Airy patterns A′ and B′, with their complex amplitude:

$$U_A(w) = \frac{2J_1(kaw)}{kaw}, \quad U_B = \frac{2J_1(kaw_1 - kaw)}{k(w_1 - w)w}. \tag{3}$$

Here kaw indicates a unit-less coordinate, i.e., the spatial dimension normalized by the system resolution. $J_1()$ is the first-order Bessel function. In an incoherent microscope, there is a linear relation between the optical intensity emitted from the sample and the intensity detected at the image plane. Therefore, we have the superimposed intensity:

$$I_{in}(w) = \left[\frac{2J_1(kaw)}{kaw}\right]^2 + \left[\frac{2J_1(kaw_1 - kaw)}{k(w_1 - w)w}\right]^2, \tag{4}$$

In a coherent microscope, a linear relation holds between the input complex amplitude and the output complex amplitude, and the two output Airy patterns A′ and B′ are considered coherent. The resultant image corresponds to the coherent superposition of the two Airy diffraction patterns. The intensity at a point situated between A′ and B′ at distance w_1 from A′ is given by:

$$I_{co}(w) = \left[\frac{2J_1(kaw)}{kaw} + \frac{2J_1[ka(w_1 - w)]}{k(w_1 - w)w} \cdot \exp(i\varphi_{diff})\right]^2. \tag{5}$$

Here, φ_{diff} denotes the phase difference between point A and B. Figure 15(b-d) compares the imaging process of two points A and B, which are separated by a Rayleigh distance (0.61λ/NA), for the case of incoherent and coherent imaging. For this purpose, the intensity distributions were calculated with Equation (4) (for incoherent microscopy) and Equation (5) (for coherent microscopy), and the results are shown in Figures (c,d), respectively. In incoherent microscopy (Figure 15(c)), A′ and B′ are considered to be resolved since the principal intensity maximum of the pattern A′ coincided with the first minimum of the pattern B′. The intensity at the midpoint between the two maxima is then equal to 0.735 of the maximum intensity of each pattern, i.e., $I(w_1)=0.735I(0)$. In coherent microscopy (Figure 15(d)), the same points, A and B separated with the same Rayleigh distance (0.61λ/NA), are considered for the following two cases: A and B having phase difference $\varphi_{diff}=0$ (in-phase) and $\varphi_{diff}=\pi$ (anti-phase) in-between. It is found from Figure 15(d) that, for the case with $\varphi_{diff}=0$ (in-phase), the Airy patterns of A′ and B′ are considered not being resolved, since a central lobe appears in the middle of the two points. However, for the case with $\varphi_{diff}=\pi$ (anti-phase), the Airy patterns of A′ and B′ are widely separated, and considered being resolved well. This implies that there is no easy criterion to evaluate the resolution of coherent microscopy, considering the resolution depends on both the microscope and sample (phase dependent). Nevertheless, we recommend to use δ

 doi:10.20944/preprints201803.0273.v1

=0.82λ/NA [58,59] to estimate the resolving power of coherent microscopy, since with this distance δ two in-phase points A and B (φ_{diff}=0) can be resolved, i.e., the intensity maximum of Airy pattern A′ coincided with the first minimum of Airy pattern B′. To transparently and reliably assess the merits of coherent microscope techniques, a practical unambiguous resolution standard (Table 1) has been proposed, considering phase dependent resolution, the presence of computational post-processing and noise [243].

Table 1 Practice guidelines for resolution determination

1. Report the predicted non-zero area of the coherent transfer function based on a specific system specifications.
2. Explicitly provide information on any a priori assumptions applied to the sample (for example, sparsity) and post-processing steps applied to the data (for example, deconvolution).
3. Image the Siemens-star target and report its amplitude and/or phase.
4. Summarize performance with the minimum periodicity metric, if desired.
5. For wide-field systems, present data for different locations across the sample plane.

7. Discussion and Conclusions

Quantitative phase microscopy (QPM), via interferometric approaches or non-interferometric approaches, provides not only high-contrast images of transparent samples, but also quantitative evaluation on their 3-D profiles or refractive index distributions. However, conventional QPM has a limited space-bandwidth product (SBP) of the optical system and consequently, trade-offs between the spatial resolution and field of view (FOV) are often needed to be made.

For the purpose of enhancement of SBP, the improvement of the spatial resolution of QPM for a fixed FOV have been performed by using a short wavelength, or synthesizing a larger hologram (for lensless QPM) or a larger numerical aperture (for lens-based QPM). Specifically speaking, in lensless QPM, moving the CCD camera or the sample was used to synthesize a larger hologram. In lens-based QPM, oblique illumination, structured illumination, and speckle illumination were used to synthesize a larger numerical aperture to improve the spatial resolution.

It is worthy to note that, the word "super-resolution" was often used for the approaches reviewed in this paper. Considering plane wave illumination and for air-immersed imaging systems, the NA is defined by the imaging lens itself and equals to a maximum theoretical value of 1 meaning that the resolution limit δ can go down to a minimum value of δ=0.82λ. However, it is habitual in microscopy to use lower NA values because these lenses provide attractive additional properties (longer working distances, larger fields of view, reduced prices…). In this case, optical "super-resolution" relates with the capability to overcome the resolution limit imposed by diffraction without changing the NA value of the lenses [244]. That is, to overcome the limitation imposed by δ =0.82λ/NA. Nevertheless and for clarification, the word "super-resolution" is attributed in other disciplines in microscopy to surpass the resolution designed by a specific microscope, i.e., 0.61λ/NA, rather than the physical limit λ/2 imposed by the Abbe diffraction limit which was obtained by integrating in phase all the diffracted waves from a sample with the angle range [0, 180°] in the semi-plane [245]. Whatever the nomenclature, the resolution-enhancement (or superresolution)

approaches described in this review yield no resolution enhancement over the Abbe diffraction limit [125].

Acknowledgments: This research was partially supported by National Science Foundation of China (NSFC) (61475187, 61605150, U1304617); Project funded by China Postdoctoral Science Foundation (2017M610623), and the Fundamental Research Funds for the Central Universities under Grants No. JB160511, XJS16005 and JBG160502. Also, part of this work was supported by the Spanish Ministerio de Economía y Competitividad and Fondo Europeo de Desarrollo Regional under the projects FIS2007-60626, FIS2010-16646, FIS2013-47548-P and FIS2017-89748-P.

Author Contributions: The authors contributed equally to this work, and all the authors wrote this paper.

Conflicts of Interest: The authors declare no conflict of interest.

References

1. Hell, S.W., Far-field optical nanoscopy. *Science* **2007**, *316*, 1153-1158.
2. Betzig, E.; Patterson, G.H.; Sougrat, R.; Lindwasser, O.W.; Olenych, S.; Bonifacino, J.S.; Davidson, M.W.; Lippincott-Schwartz, J.; Hess, H.F., Imaging intracellular fluorescent proteins at nanometer resolution. *Science* **2006**, *313*, 1642-1645.
3. Gao, P.; Prunsche, B.; Zhou, L.; Nienhaus, K.; Nienhaus, G.U., Background suppression in fluorescence nanoscopy with stimulated emission double depletion. *Nat. Photon.* **2017**, *11*, 163-169.
4. Kemper, B.; Carl, D.; Schnekenburger, J.; Bredebusch, I.; Schafer, M.; Domschke, W.; von Bally, G., Investigation of living pancreas tumor cells by digital holographic microscopy. *J. Biomed. Opt.* **2006**, *11*, 34005.
5. Pavillon, N.; Kuhn, J.; Moratal, C.; Jourdain, P.; Depeursinge, C.; Magistretti, P.J.; Marquet, P., Early cell death detection with digital holographic microscopy. *Plos One* **2012**, *7*. e30912.
6. Mir, M.; Babacan, S.D.; Bednarz, M.; Do, M.N.; Golding, I.; Popescu, G., Visualizing escherichia coli sub-cellular structure using sparse deconvolution spatial light interference tomography. *Plos One* **2012**, *7*. e39816.
7. Platt, B.C.; Shack, R., History and principles of shack-hartmann wavefront sensing. *J. Refract. Surg.* **2001**, *17*, S573-S577.
8. Costa, J.B., Modulation effect of the atmosphere in a pyramid wave-front sensor. *Appl. Opt.* **2005**, *44*, 60-66.
9. Goodman, J.W.; Lawrence, R.W., Digital image formation from electronically detected holograms. *Appl. Phys. Lett.* **1967**, *11*, 77-79.
10. Cuche, E.; Marquet, P.; Depeursinge, C., Spatial filtering for zero-order and twin-image elimination in digital off-axis holography. *Appl. Opt.* **2000**, *39*, 4070-4075.
11. Kemper, B.; von Bally, G., Digital holographic microscopy for live cell applications and technical inspection. *Appl. Opt.* **2008**, *47*, A52-A61.
12. Osten, W.; Faridian, A.; Gao, P.; Körner, K.; Naik, D.; Pedrini, G.; Singh, A.K.; Takeda, M.; Wilke, M., Recent advances in digital holography [invited]. *Appl. Opt.* **2014**, *53*, G44-G63.

13. Langehanenberg, P.; Kemper, B.; Dirksen, D.; von Bally, G., Autofocusing in digital holographic phase contrast microscopy on pure phase objects for live cell imaging. *Appl. Opt.* **2008**, *47*, D176-182.
14. Mann, C.; Yu, L.; Lo, C.; Kim, M., High-resolution quantitative phase-contrast microscopy by digital holography. *Opt. Express* **2005** *13*, 8693-8698..
15. Pedrini, G.; Froning, P.; Tiziani, H.J.; Gusev, M.E., Pulsed digital holography for high-speed contouring that uses a two-wavelength method. *Appl. Opt.* **1999**, *38*, 3460-3467.
16. Popescu, G.; Deflores, L.P.; Vaughan, J.C.; Badizadegan, K.; Iwai, H.; Dasari, R.R.; Feld, M.S., Fourier phase microscopy for investigation of biological structures and dynamics. *Opt. Lett.* **2004**, *29*, 2503-2505.
17. Antkowiak, M.; Callens, N.; Yourassowsky, C.; Dubois, F., Extended focused imaging of a microparticle field with digital holographic microscopy. *Opt. Lett.* **2008**, *33*, 1626-1628.
18. Fatih Toy, M.; Kühn, J.; Richard, S.; Parent, J.; Egli, M.; Depeursinge, C., Accelerated autofocusing of off-axis holograms using critical sampling. *Opt. Lett.* **2012**, *37*, 5094-5096.
19. Ferraro, P.; De Nicola, S.; Coppola, G.; Finizio, A.; Alfieri, D.; Pierattini, G., Controlling image size as a function of distanceand wavelength in fresnel-transformreconstruction of digital holograms. *Opt. Lett.* **2004.4**, *29*, 854-856.
20. Bhaduri, B.; Pham, H.; Mir, M.; Popescu, G., Diffraction phase microscopy with white light. *Opt. Lett.* **2012**, *37*, 1094-1096.
21. Zheng, J.J.; Gao, P.; Shao, X.P., Opposite-view digital holographic microscopy with autofocusing capability. *Sci. Rep.* **2017**, *7*.
22. Lyu, M.; Yuan, C.J.; Li, D.Y.; Situ, G.H., Fast autofocusing in digital holography using the magnitude differential. *Appl. Opt.* **2017**, *56*, F152-F157.
23. Gao, P.; Harder, I.; Nercissian, V.; Mantel, K.; Yao, B.L., Phase-shifting point-diffraction interferometry with common-path and in-line configuration for microscopy. *Opt. Lett.* **2010**, *35*, 712-714.
24. Guo, R.L.; Yao, B.L.; Gao, P.; Min, J.W.; Zhou, M.L.; Han, J.; Yu, X.; Yu, X.H.; Lei, M.; Yan, S.H., *et al.*, Off-axis digital holographic microscopy with led illumination based on polarization filtering. *Appl. Opt.* **2013**, *52*, 8233-8238.
25. Gao, P.; Yao, B.L.; Lindlein, N.; Mantel, K.; Harder, I.; Geist, E., Phase-shift extraction for generalized phase-shifting interferometry. *Opt. Lett.* **2009**, *34*, 3553-3555.
26. Gao, P.; Yao, B.L.; Min, J.W.; Guo, R.L.; Zheng, J.J.; Ye, T.; Harder, I.; Nercissian, V.; Mantel, K., Parallel two-step phase-shifting point-diffraction interferometry for microscopy based on a pair of cube beamsplitters. *Opt. Express* **2011**, *19*, 1930-1935.
27. Picazo-Bueno, J.A.; Cojoc, D.; Iseppon, F.; Torre, V.; Mico, V., Single-shot, dual-mode, water-immersion microscopy platform for biological applications. *Appl. Opt.* **2018**, *57*, A242-A249.
28. Pedrini, G.; Osten, W.; Zhang, Y., Wave-front reconstruction from a sequence of interferograms recorded at different planes. *Opt. Lett.* **2005**, *30*, 833-835.
29. Almoro, P.; Pedrini, G.; Osten, W., Complete wavefront reconstruction using sequential intensity measurements of a volume speckle field. *Appl. Opt.s* **2006**, *45*, 8596-8605.
30. Rodenburg, J.M.; Faulkner, H.M.L., A phase retrieval algorithm for shifting illumination. *Appl. Phys. Lett.* **2004**, *85*, 4795-4797.

31. Zhang, F.C.; Pedrini, G.; Osten, W., Phase retrieval of arbitrary complex-valued fields through aperture-plane modulation. *Phys. Rev. A* **2007**, *75*. 043805.
32. Gao, P.; Pedrini, G.; Osten, W., Phase retrieval with resolution enhancement by using structured illumination. *Opt. Lett.* **2013**, *38*, 5204-5207.
33. Sanz, M.; Picazo-Bueno, J.A.; Granero, L.; Garcia, J.; Mico, V., Compact, cost-effective and field-portable microscope prototype based on mishelf microscopy. *Sci Rep.* **2017**, *7*. 43291.
34. Noom, D.W.E.; Eikema, K.S.E.; Witte, S., Lensless phase contrast microscopy based on multiwavelength fresnel diffraction. *Opt. Lett.* **2014**, *39*, 193-196.
35. Noom, D.W.E.; Flaes, D.E.B.; Labordus, E.; Eikema, K.S.E.; Witte, S., High-speed multi-wavelength fresnel diffraction imaging. *Opt. Express* **2014**, *22*, 30504-30511.
36. Sanz, M.; Picazo-Bueno, J.A.; Garcia, J.; Mico, V., Improved quantitative phase imaging in lensless microscopy by single-shot multi-wavelength illumination using a fast convergence algorithm. *Opt. Express* **2015**, *23*, 21352-21365.
37. Lohmann, A.W.; Dorsch, R.G.; Mendlovic, D.; Zalevsky, Z.; Ferreira, C., Space-bandwidth product of optical signals and systems. *J. Opt. Soc. Am. A* **1996**, *13*, 470-473.
38. Cox, I.J.; Sheppard, C.J.R., Information capacity and resolution in an optical-system. *J. Opt. Soc. Am. A* **1986**, *3*, 1152-1158.
39. Zheng, G.A.; Horstmeyer, R.; Yang, C.H., Wide-field, high-resolution fourier ptychographic microscopy. *Nat. Photon.* **2013**, *7*, 739-745.
40. Mendlovic, D.; Lohman, A.W., Sw-adaptation and its application for super resolution: Fundamentals. *J. Opt. Soc. Am. A* **1997**, *14*, 558-562.
41. Mendlovic, D.; Lohman, A.W.; Zalevsky, Z., Sw-adaptation and its application for super resolution: Examples. *J. Opt. Soc. Am. A* **2009**, *14*, 562-567.
42. Micó, V.; Zalevsky, Z.; García, J., Optical superresolution: Imaging beyond abbe's diffraction limit. *Speckle* **2009**, *5*, 110-123.
43. Zalevsky, Z.; Mico, V.; Garcia, J., Nanophotonics for optical super resolution from an information theoretical perspective: A review. *J. Nanophotonics* **2009**, *3*.
44. Bon, P.; Aknoun, S.; Monneret, S.; Wattellier, B., Enhanced 3D spatial resolution in quantitative phase microscopy using spatially incoherent illumination. *Opt. Express* **2014**, *22*, 8654-8671.
45. Guo, R.L.; Wang, F., Compact and stable real-time dual-wavelength digital holographic microscopy with a long-working distance objective. *Opt. Express* **2017**, *25*, 24512-24520.
46. Rappaz, B.; Marquet, P.; Cuche, E.; Emery, Y.; Depeursinge, C.; Magistretti, P.J., Measurement of the integral refractive index and dynamic cell morphometry of living cells with digital holographic microscopy. *Opt. Express* **2005**, *13*, 9361-9373.
47. Belashov, A.V.; Zhikhoreva, A.A.; Bespalov, V.G.; Novik, V.I.; Zhilinskaya, N.T.; Semenova, I.V.; Vasyutinskii, O.S., Refractive index distributions in dehydrated cells of human oral cavity epithelium. *J. Opt. Soc. Am. B* **2017**, *34*, 2538-2543.
48. Zheng, J.J.; Gao, P.; Shao, X.P.; Nienhaus, G.U., Refractive index measurement of suspended cells using opposed-view digital holographic microscopy. *Appl. Opt.* **2017**, *56*, 9000-9005.
49. Kim, M.; Choi, Y.; Fang-Yen, C.; Sung, Y.; Dasari, R.R.; Feld, M.S.; Choi, W., High-speed synthetic aperture microscopy for live cell imaging. *Opt. Lett.* **2011**, *36*, 148-150.

50. Kemper, B.; Kosmeier, S.; Langehanenberg, P.; von Bally, G.; Bredebusch, I.; Domschke, W.; Schnekenburger, J., Integral refractive index determination of living suspension cells by multifocus digital holographic phase contrast microscopy. *J. Biomed. Opt.* **2007**, *12*, 054009.
51. Zheng, J.J.; Yang, Y.L.; Lei, M.; Yao, B.L.; Gao, P.; Ye, T., Fluorescence volume imaging with an axicon: Simulation study based on scalar diffraction method. *Appl. Opt.* **2012**, *51*, 7236-7245.
52. Wu, G.F.; Wang, F.; Cai, Y.J., Generation and self-healing of a radially polarized bessel-gauss beam. *Phys. Rev. A* **2014**, *89*.
53. Zheng, J.J.; Yao, B.L.; Yang, Y.L.; Lei, M.; Gao, P.; Li, R.Z.; Yan, S.H.; Dan, D.; Ye, T., Investigation of bessel beam propagation in scattering media with scalar diffraction method. *Chin. Opt. Lett.* **2013**, *11*.
54. Zheng, J.J.; Gao, P.; Shao, X.P., Aberration compensation and resolution improvement of focus modulation microscopy. *J. Opt.* **2017**, *19*.
55. Garcia-Sucerquia, J.; Xu, W.; Jericho, S.K.; Jericho, M.H.; Kreuzer, H.J., 4-d imaging of fluid flow with digital in-line holographic microscopy. *Optik* **2008**, *119*, 419-423.
56. Katz, J.; Sheng, J., Applications of holography in fluid mechanics and particle dynamics. *Annu. Rev. Fluid. Mech.* **2010**, *42*, 531-555.
57. Marx, V., Microscopy: Hello, adaptive optics. *Nat. Methods* **2017**, *14*, 1133-1136.
58. Cotte, Y.; Toy, F.; Jourdain, P.; Pavillon, N.; Boss, D.; Magistretti, P.; Marquet, P.; Depeursinge, C., Marker-free phase nanoscopy. *Nat. Photon.* **2013**, *7*, 418-418.
59. denDekker, A.J.; vandenBos, A., Resolution: A survey. *J. Opt. Soc. Am. A* **1997**, *14*, 547-557.
60. Faridian, A.; Hopp, D.; Pedrini, G.; Eigenthaler, U.; Hirscher, M.; Osten, W., Nanoscale imaging using deep ultraviolet digital holographic microscopy. *Opt. Express* **2010**, *18*, 14159-14164.
61. Pedrini, G.; Zhang, F.C.; Osten, W., Digital holographic microscopy in the deep (193 nm) ultraviolet. *Appl. Opt.* **2007**, *46*, 7829-7835.
62. Micó, V.; Ferreira, C.; García, J., Surpassing digital holography limits by lensless object scanning holography. *Opt. Express* **2012**, *20*, 9382-9395.
63. Le Clerc, F.; Gross, M.; Collot, L., Synthetic-aperture experiment in the visible with on-axis digital heterodyne holography. *Opt. Lett.* **2001**, *26*, 1550-1552.
64. Paturzo, M.; Ferraro, P., Correct self-assembling of spatial frequencies in super-resolution synthetic aperture digital holography. *Opt. Lett.* **2009**, *34*, 3650-3652.
65. Schwarz, C.J.; Kuznetsova, Y.; Brueck, S.R.J., Imaging interferometric microscopy. *Opt. Lett.* **2003**, *28*, 1424-1426.
66. Neumann, A.; Kuznetsova, Y.; Brueck, S.R., Structured illumination for the extension of imaging interferometric microscopy. *Opt. Express* **2008**, *16*, 6785-6793.
67. Lai, X.J.; Tu, H.Y.; Lin, Y.C.; Cheng, C.J., Coded aperture structured illumination digital holographic microscopy for superresolution imaging. *Opt. Lett.* **2018**, *43*, 1143-1146.
68. Chowdhury, S.; Izatt, J., Structured illumination diffraction phase microscopy for broadband, subdiffraction resolution, quantitative phase imaging. *Opt. Lett.* **2014**, *39*, 1015-1018.

69. Zheng, J.J.; Gao, P.; Yao, B.L.; Ye, T.; Lei, M.; Min, J.W.; Dan, D.; Yang, Y.L.; Yan, S.H., Digital holographic microscopy with phase-shift-free structured illumination. *Photo. Res.* **2014**, *2*, 87-91.
70. Yeh, L.H.; Tian, L.; Waller, L., Structured illumination microscopy with unknown patterns and a statistical prior. *Biomed. Opt. Express* **2017**, *8*, 695-711.
71. Ganjkhani, Y.; Charsooghi, M.A.; Akhlaghi, E.A.; Moradi, A.R., Super-resolved mirau digital holography by structured illumination. *Opt. Commun.* **2017**, *404*, 110-117.
72. Zalevsky, Z.; Garcia, J.; Mico, V., Transversal superresolution with noncontact axial movement of periodic structures. *J. Opt. Soc. Am. A* **2007**, *24*, 3220-3225.
73. García, J.; Micó, V.; Cojoc, D.; Zalevsky, Z., Full field of view super-resolution imaging based on two static gratings and white light illumination. *Appl. Opt.* **2008**, *47*, 3080-3087.
74. Mico, V.; Limon, O.; Gur, A.; Zalevsky, Z.; Garcia, J., Transverse resolution improvement using rotating-grating time-multiplexing approach. *J. Opt. Soc. Am. A* **2008**, *25*, 1115-1129.
75. Wilde, J.P.; Goodman, J.W.; Eldar, Y.C.; Takashima, Y., Coherent superresolution imaging via grating-based illumination. *Appl. Opt.* **2017**, *56*, A79-A88.
76. Park, Y.; Choi, W.; Yaqoob, Z.; Dasari, R.; Badizadegan, K.; Feld, M.S., Speckle-field digital holographic microscopy. *Opt. Express* **2009**, *17*, 12285-12292.
77. García, J.; Zalevsky, Z.; Fixler, D., Synthetic aperture superresolution by speckle pattern projection. *Opt. Express* **2005**, *13*, 6073-6078.
78. Zalevsky, Z.; Fish, E.; Shachar, N.; Vexberg, Y.; Mico, V.; Garcia, J., Super-resolved imaging with randomly distributed, time- and size-varied particles. *J. Opt. a-Pure Appl. Op* **2009**, *11*.085406.
79. Sylman, D.; Mico, V.; Garcia, J.; Zalevsky, Z., Random angular coding for superresolved imaging. *Appl. Opt.* **2010**, *49*, 4874-4882.
80. Zheng, J.J.; Pedrini, G.; Gao, P.; Yao, B.L.; Osten, W., Autofocusing and resolution enhancement in digital holographic microscopy by using speckle-illumination. *J. Opt.* **2015**, *17*. 085301.
81. Wagner, O.; Schwarz, A.; Shemer, A.; Ferreira, C.; Garcia, J.; Zalevsky, Z., Superresolved imaging based on wavelength multiplexing of projected unknown speckle patterns. *Appl. Opt.* **2015**, *54*, D51-D60.
82. Trujillo, C. A.; Garcia-Sucerquia, J., Automatic method for focusing biological specimens in digital lensless holographic microscopy, *Opt. Lett.* **2014**, 39, 2569-2572.
83. Gao, P.; Yao, B.L.; Rupp, R.; Min, J.W.; Guo, R.L.; Ma, B.H.; Zheng, J.J.; Lei, M.; Yan, S.H.; Dan, D., *et al.*, Autofocusing based on wavelength dependence of diffraction in two-wavelength digital holographic microscopy. *Opt. Lett.* **2012**, *37*, 1172-1174.
84. Gao, P.; Yao, B.L.; Min, J.W.; Guo, R.L.; Ma, B.H.; Zheng, J.J.; Lei, M.; Yan, S.H.; Dan, D.; Ye, T., Autofocusing of digital holographic microscopy based on off-axis illuminations. *Opt. Lett.* **2012**, *37*, 3630-3632.
85. Sato, T.; Ueda, M.; Ikeda, T., Real-time superresolution by means of an ultrasonic light diffractor and tv system. *Appl. Opt.* **1974**, *13*, 1318-1321.
86. Sato, T.; Ueda, M.; Yamagish.G, Superresolution microscope using electrical superposition of holograms. *Appl. Opt.* **1974**, *13*, 406-408.

87. Ueda, M.; Sato, T.; Kondo, M., Superresolution by multiple superposition of image holograms having different carrier frequencies. *Opt. Acta.* **1973**, *20*, 403-410.
88. Ueda, M.; Sato, T., Superresolution by holography. *J. Opt. Soc. Am.* **1971**, *61*, 418-&.
89. Mico, V.; Zalevsky, Z.; Garcia, J., Superresolved common-path phase-shifting digital inline holographic microscopy using a spatial light modulator. *Opt. Lett.* **2012**, *37*, 4988-4990.
90. Kuznetsova, Y.; Neumann, A.; Brueck, S.R.J., Imaging interferometric microscopy. *J. Opt. Soc. Am. A* **2008**, *25*, 811-822.
91. Mico, V.; Zalevsky, Z.; García-Martínez, P.; García, J., Synthetic aperture superresolution with multiple off-axis holograms. *J. Opt. Soc. Am. A* **2006**, *23*, 3162-3170.
92. Picazo-Bueno, J.A.; Zalevsky, Z.; Garcia, J.; Mico, V., Superresolved spatially multiplexed interferometric microscopy. *Opt. Lett.* **2017**, *42*, 927-930.
93. Yuan, C.J.; Situ, G.; Pedrini, G.; Ma, J.; Osten, W., Resolution improvement in digital holography by angular and polarization multiplexing. *Appl. Opt.* **2011**, *50*, B6-B11.
94. Choi, Y.; Kim, M.; Yoon, C.; Yang, T.D.; Lee, K.J.; Choi, W., Synthetic aperture microscopy for high resolution imaging through a turbid medium. *Opt. Lett.* **2011**, *36*, 4263-4265.
95. Calabuig, A.; Garcia, J.; Ferreira, C.; Zalevsky, Z.; Mico, V., Resolution improvement by single-exposure superresolved interferometric microscopy with a monochrome sensor. *J. Opt. Soc. Am. A* **2011**, *28*, 2346-2358.
96. Calabuig, A.; Micó, V.; Garcia, J.; Zalevsky, Z.; Ferreira, C., Single-exposure super-resolved interferometric microscopy by red–green–blue multiplexing. *Opt. Lett.* **2011** *36*, 885-887.
97. Granero, L.; Ferreira, C.; Zalevsky, Z.; Garcia, J.; Mico, V., Single-exposure super-resolved interferometric microscopy by rgb multiplexing in lensless configuration. *Opt. Laser Eng.* **2016**, *82*, 104-112.
98. Gutzler, T.; Hillman, T.R.; Alexandrov, S.A.; Sampson, D.D., Coherent aperture-synthesis, wide-field, high-resolution holographic microscopy of biological tissue. *Opt. Lett.* **2010**, *35*, 1136-1138.
99. Buhl, J.; Babovsky, H.; Kiessling, A.; Kowarschik, R., Digital synthesis of multiple off-axis holograms with overlapping fourier spectra. *Opt. Commun.* **2010**, *283*, 3631-3638.
100. Hillman, T.R.; Gutzler, T.; Alexandrov, S.A.; Sampson, D.D., High-resolution, wide-field object reconstruction with synthetic aperture fourier holographic optical microscopy. *Opt. Express* **2009**, *17*, 7873-7892.
101. Mico, V.; Zalevsky, Z.; Ferreira, C.; Garcia, J., Superresolution digital holographic microscopy for three-dimensional samples. *Opt. Express* **2008**, *16*, 19260-19270.
102. Neumann, A.; Kuznetsova, Y.; Brueck, S.R.J., Optical resolution below lambda/4 using synthetic aperture microscopy and evanescent-wave illumination. *Opt. Express* **2008**, *16*, 20477-20483.
103. Kuznetsova, Y.; Neumann, A.; Brueck, S.R.J., Imaging interferometric microscopy. *J. Opt. Soc. Am. A* **2008**, *25*, 811-822.
104. Indebetouw, G.; Tada, Y.; Rosen, J.; Brooker, G., Scanning holographic microscopy with resolution exceeding the rayleigh limit of the objective by superposition of off-axis holograms. *Appl. Opt.* **2007**, *46*, 993-1000.
105. Mico, V.; Zalevsky, Z.; Garcia, J., Synthetic aperture microscopy using off-axis illumination and polarization coding. *Opt. Commun.* **2007**, *276*, 209-217.

106. Kuznetsova, Y.; Neumann, A.; Brueck, S.R.J., Imaging interferometric microscopy - approaching the linear systems limits of optical resolution. *Opt. Express* **2007**, *15*, 6651-6663.
107. Alexandrov, S.A.; Hillman, T.R.; Gutzler, T.; Sampson, D.D., Synthetic aperture fourier holographic optical microscopy. *Phys. Rev. Lett.* **2006**, *97*.168102.
108. Mico, V.; Zalevsky, Z.; Garcia, J., Superresolution optical system by common-path interferometry. *Opt. Express* **2006**, *14*, 5168-5177.
109. Mico, V.; Zalevsky, Z.; Garcia-Martinez, P.; Garcia, J., Superresolved imaging in digital holography by superposition of tilted wavefronts. *Appl. Opt.* **2006**, *45*, 822-828.
110. Mico, V.; Zalevsky, Z.; Garcia-Martinez, P.; Garcia, J., Synthetic aperture superresolution with multiple off-axis holograms. *J. Opt. Soc. Am. A* **2006**, *23*, 3162-3170.
111. Indebetouw, G.; El Maghnouji, A.; Foster, R., Scanning holographic microscopy with transverse resolution exceeding the rayleigh limit and extended depth of focus. *J. Opt. Soc. Am. A* **2005**, *22*, 892-898.
112. Indebetouw, G.; Tada, Y.; Rosen, J.; Brooker, G., Scanning holographic microscopy with resolution exceeding the Rayleigh limit of the objective by superposition of off-axis holograms. *Appl. Opt.* **2007** *46*, 993-1000.
113. Mico, V.; Zalevsky, Z.; Garcia-Martinez, P.; Garcia, J., Single-step superresolution by interferometric imaging. *Opt. Express* **2004**, *12*, 2589-2596.
114. Lai, X.-J.; Tu, H.-Y.; Wu, C.-H.; Lin, Y.-C.; Cheng, C.-J., Resolution enhancement of spectrum normalization in synthetic aperture digital holographic microscopy. *Appl. Opt.* **2015** *54*, A51-A58.
115. Choi, Y.; Kim, M.; Yoon, C.; Yang, T.D.; Lee, K.J.; Choi, W., Synthetic aperture microscopy for high resolution imaging through a turbid medium. *Opt. Lett.* **2011**, *36*, 4263-4265.
116. Lee, D.J.; Weiner, A.M., Optical phase imaging using a synthetic aperture phase retrieval technique. *Opt. Express* **2014**, *22*, 9380-9394.
117. Kim, M.; Choi, Y.; Fang-Yen, C.; Sung, Y.; Kim, K.; Dasari, R.R.; Feld, M.S.; Choi, W., Three-dimensional differential interference contrast microscopy using synthetic aperture imaging. *J. Biomed. Opt.* **2012**, *17*.
118. Gao, P.; Yao, B.L.; Harder, I.; Lindlein, N.; Torcal-Milla, F.J., Phase-shifting zernike phase contrast microscopy for quantitative phase measurement. *Opt. Lett.* **2011**, *36*, 4305-4307.
119. Mico, V.; Garcia, J.; Zalevsky, Z., Axial superresolution by synthetic aperture generation. *J. Opt. a-Pure Appl. Op.* **2008**, *10*.
120. Micó, V.; Zalevsky, Z.; García, J., Edge processing by synthetic aperture superresolution in digital holographic microscopy. *3D Research* **2011**, *2*, 01001.
121. Mico, V., Zalevsky, Z.; Garcia, J., Common-path phase-shifting digital holographic microscopy: A way to quantitative phase imaging and superresolution. *Opt. Commun.* **2008**, *281*, 4273-4281.
122. Gustafsson, M.G.L., Surpassing the lateral resolution limit by a factor of two using structured illumination microscopy. *J Microsc-Oxford* **2000**, *198*, 82-87.
123. Gustafsson, M.G.L., Nonlinear structured-illumination microscopy: Wide-field fluorescence imaging with theoretically unlimited resolution. *PNAS* **2005**, *102*, 13081-13086.

124. Gao, P.; Pedrini, G.; Osten, W., Structured illumination for resolution enhancement and autofocusing in digital holographic microscopy. *Opt. Lett.* **2013**, *38*, 1328-1330.
125. Wicker, K.; Heintzmann, R., Resolving a misconception about structured illumination. *Nat. Photo.* **2014**, *8*, 342-344.
126. Yuan, C.J.; Ma, J.; Dou, J.T.; Wei, J.D.; Feng, S.T.; Nie, S.P.; Chang, C.L., Resolution enhancement of the microscopic imaging by unknown sinusoidal structured illumination with iterative algorithm. *Appl. Opt.* **2017**, *56*, F78-F83.
127. Chen, J.L.; Xu, Y.; Lv, X.H.; Lai, X.M.; Zeng, S.Q., Super-resolution differential interference contrast microscopy by structured illumination. *Opt.s Express* **2013**, *21*, 112-121.
128. Somekh, M.G.; See, C.W.; Goh, J., Wide field amplitude and phase confocal microscope with speckle illumination. *Opt. Commun.* **2000**, *174*, 75-80.
129. Dubois, F.; Requena, M.L.N.; Minetti, C.; Monnom, O.; Istasse, E., Partial spatial coherence effects in digital holographic microscopy with a laser source. *Appl. Opt.* **2004**, *43*, 1131-1139.
130. Pitter, M.C.; See, C.W.; Somekh, M.G., Full-field heterodyne interference microscope with spatially incoherent illumination. *Opt. Lett.* **2004**, *29*, 1200-1202.
131. Zalevsky, Z.; Gur, E.; Garcia, J.; Mico, V.; Javidi, B., Superresolved and field-of-view extended digital holography with particle encoding. *Opt. Lett.* **2012**, *37*, 2766-2768.
132. Ilovitsh, T.; Ilovitsh, A.; Wagner, O.; Zalevsky, Z., Superresolved nanoscopy using brownian motion of fluorescently labeled gold nanoparticles. *Appl. Opt.* **2017**, *56*, 1365-1369.
133. Gur, A.; Fixler, D.; Mico, V.; Garcia, J.; Zalevsky, Z., Linear optics based nanoscopy. *Opt. Express* **2010**, *18*, 22222-22231.
134. Zalevsky, Z.; Saat, E.; Orbach, S.; Mico, V.; Garcia, J., Exceeding the resolving imaging power using environmental conditions. *Appl. Opt.* **2008**, *47*, A1-A6.
135. Françon, M., Amélioration de resolution d'optique. *Nuovo. Cimento. Suppl.* **1952**, *9*, 283-290.
136. Hoang, T.X.; Duan, Y.B.; Chen, X.D.; Barbastathis, G., Focusing and imaging in microsphere-based microscopy. *Opt. Express* **2015**, *23*, 12337-12353.
137. Duan, Y.B.; Barbastathis, G.; Zhang, B.L., Classical imaging theory of a microlens with super-resolution. *Opt. Lett.* **2013**, *38*, 2988-2990.
138. Jiang, L.Y.; Zhang, W.; Yuan, H.; Li, X.Y., Super resolution from pure/hybrid nanoscale solid immersion lenses under dark-field illumination. *Opt. Express* **2016**, *24*, 25224-25232.
139. Darafsheh, A.; Guardiola, C.; Palovcak, A.; Finlay, J.C.; Carabe, A., Optical super-resolution imaging by high-index microspheres embedded in elastomers. *Opt. Lett.* **2015**, *40*, 5-8.
140. Aakhte, M.; Abbasian, V.; Akhlaghi, E.A.; Moradi, A.R.; Anand, A.; Javidi, B., Microsphere-assisted super-resolved mirau digital holographic microscopy for cell identification. *Appl. Opt.* **2017**, *56*, D8-D13.
141. Wang, Y.X.; Guo, S.; Wang, D.Y.; Lin, Q.W.; Rong, L.; Zhao, J., Resolution enhancement phase-contrast imaging by microsphere digital holography. *Opt. Commun.* **2016**, *366*, 81-87.
142. Gabor, D., A new microscopic principle. *Nature* **1948**, *161*, 777-778.
143. Xu, W.B.; Jericho, M.H.; Meinertzhagen, I.A.; Kreuzer, H.J., Digital in-line holography for biological applications. *PNAS* **2001**, *98*, 11301-11305.

144. Greenbaum, A.; Luo, W.; Su, T.W.; Gorocs, Z.; Xue, L.; Isikman, S.O.; Coskun, A.F.; Mudanyali, O.; Ozcan, A., Imaging without lenses: Achievements and remaining challenges of wide-field on-chip microscopy. *Nat. Methods* **2012**, *9*, 889-895.
145. Repetto, L.; Piano, E.; Pontiggia, C., Lensless digital holographic microscope with light-emitting diode illumination. *Opt. Lett.* **2004**, *29*, 1132-1134.
146. Jericho, S.K.; Garcia-Sucerquia, J.; Xu, W.B.; Jericho, M.H.; Kreuzer, H.J., Submersible digital in-line holographic microscope. *Rev. Sci. Instrum.* **2006**, *77*.
147. Mendoza-Yero, O.; Carbonell-Leal, M.; Lancis, J.; Garcia-Sucerouia, J., Second-harmonic illumination to enhance multispectral digital lensless holographic microscopy. *Opt. Lett.* **2016**, *41*, 1062-1065.
148. Seo, S.; Su, T.W.; Erlinger, A.; Ozcan, A., Multi-color lucas: Lensfree on-chip cytometry using tunable monochromatic illumination and digital noise reduction. *Cell Mol Bioeng* **2008**, *1*, 146-156.
149. Ozcan, A.; Demirci, U., Ultra wide-field lens-free monitoring of cells on-chip. *Lab. Chip.* **2008**, *8*, 98-106.
150. Lee, S.A.; Erath, J.; Zheng, G.A.; Ou, X.Z.; Willems, P.; Eichinger, D.; Rodriguez, A.; Yang, C.H., Imaging and identification of waterborne parasites using a chip-scale microscope. *Plos One* **2014**, *9*. e89712.
151. Kazemzadeh, F.; Wong, A., Laser light-field fusion for wide-field lensfree on-chip phase contrast microscopy of nanoparticles. *Sci. Rep.* **2016**, *6*. 38981.
152. Jiang, H.Z.; Zhao, J.L.; Di, J.L., Digital color holographic recording and reconstruction using synthetic aperture and multiple reference waves. *Opt. Commun.* **2012**, *285*, 3046-3049.
153. Tippie, A.E.; Kumar, A.; Fienup, J.R., High-resolution synthetic-aperture digital holography with digital phase and pupil correction. *Opt. Express* **2011**, *19*, 12027-12038.
154. Li, H.Y.; Zhong, L.Y.; Ma, Z.J.; Lu, X.X., Joint approach of the sub-holograms in on-axis lensless fourier phase-shifting synthetic aperture digital holography. *Opt. Commun.* **2011**, *284*, 2268-2272.
155. Lim, S.; Choi, K.; Hahn, J.; Marks, D.L.; Brady, D.J., Image-based registration for synthetic aperture holography. *Opt. Express* **2011**, *19*, 11716-11731.
156. Claus, D., High resolution digital holographic synthetic aperture applied to deformation measurement and extended depth of field method. *Appl. Opt.* **2010**, *49*, 3187-3198.
157. Katz, B.; Rosen, J., Super-resolution in incoherent optical imaging using synthetic aperture with fresnel elements. *Opt. Express* **2010**, *18*, 962-972.
158. Jiang, H.Z.; Zhao, J.L.; Di, J.L.; Qin, C.A., Numerically correcting the joint misplacement of the sub-holograms in spatial synthetic aperture digital fresnel holography. *Opt. Express* **2009**, *17*, 18836-18842.
159. Mico, V.; Granero, L.; Zalevsky, Z.; Garcia, J., Superresolved phase-shifting gabor holography by ccd shift. *J. Opt. a-Pure. Appl. Op.* **2009**, *11*, 125408.
160. Martinez-Leon, L.; Javidi, B., Synthetic aperture single-exposure on-axis digital holography. *Opt. Express* **2008**, *16*, 161-169.
161. Di, J.L.; Zhao, J.L.; Jiang, H.Z.; Zhang, P.; Fan, Q.; Sun, W.W., High resolution digital holographic microscopy with a wide field of view based on a synthetic aperture technique and use of linear ccd scanning. *Appl. Opt.* **2008**, *47*, 5654-5659.

162. Almoro, P.; Pedrini, G.; Osten, W., Aperture synthesis in phase retrieval using a volume-speckle field. *Opt. Lett.* **2007**, *32*, 733-735.
163. Massig, J.H., Digital off-axis holography with a synthetic aperture. *Opt. Lett.* **2002**, *27*, 2179-2181.
164. Le Clerc, F.; Gross, M.; Collot, L., Synthetic-aperture experiment in the visible with on-axis digital heterodyne holography. *Opt. Lett.* **2001**, *26*, 1550-1552.
165. Thurman, S.T.; Bratcher, A., Multiplexed synthetic-aperture digital holography. *Appl Opt.* **2015**, *54*, 559-568.
166. Mico, V.; Zalevsky, Z.; Garcia, J., Superresolved common-path phase-shifting digital inline holographic microscopy using a spatial light modulator. *Opt. Lett.* **2012**, *37*, 4988-4990.
167. Granero, L.; Zalevsky, Z.; Mico, V., Single-exposure two-dimensional superresolution in digital holography using a vertical cavity surface-emitting laser source array. *Opt. Lett.* **2011**, *36*, 1149-1151.
168. Zhao, J.L.; Yan, X.B.; Sun, W.W.; Di, J.L., Resolution improvement of digital holographic images based on angular multiplexing with incoherent beams in orthogonal polarization states. *Opt. Lett.* **2010**, *35*, 3519-3521.
169. Mico, V.; Zalevsky, Z., Superresolved digital in-line holographic microscopy for high-resolution lensless biological imaging. *J. Biomed. Opt.* **2010**, *15*.
170. Granero, L.; Mico, V.; Zalevsky, Z.; Garcia, J., Synthetic aperture superresolved microscopy in digital lensless fourier holography by time and angular multiplexing of the object information. *Appl. Opt.* **2010**, *49*, 845-857.
171. Feng, P.; Wen, X.; Lu, R., Long-working-distance synthetic aperture fresnel off-axis digital holography. *Opt. Express* **2009**, *17*, 5473-5480.
172. Yuan, C.J.; Zhai, H.C.; Liu, H.T., Angular multiplexing in pulsed digital holography for aperture synthesis. *Opt. Lett.* **2008**, *33*, 2356-2358.
173. Zhang, W.H.; Cao, L.C.; Jin, G.F.; Brady, D., Full field-of-view digital lens-free holography for weak-scattering objects based on grating modulation. *Appl. Opt.* **2018**, *57*, A164-A171.
174. Lin, Q.W.; Wang, D.Y.; Wang, Y.X.; Rong, L.; Chang, S.F., Super-resolution imaging in digital holography by using dynamic grating with a spatial light modulator. *Opt. Laser Eng.* **2015**, *66*, 279-284.
175. Paturzo, M.; Ferraro, P., Correct self-assembling of spatial frequencies in super-resolution synthetic aperture digital holography. *Opt. Lett.* **2009**, *34*, 3650-3652.
176. Granero, L.; Mico, V.; Zalevsky, Z.; Garcia, J., Superresolution imaging method using phase-shifting digital lensless fourier holography. *Opt. Express* **2009**, *17*, 15008-15022.
177. Paturzo, M.; Merola, F.; Grilli, S.; De Nicola, S.; Finizio, A.; Ferraro, P., Super-resolution in digital holography by a two-dimensional dynamic phase grating. *Opt. Express* **2008**, *16*, 17107-17118.
178. Hezaveh, M.S.; Riahi, M.R.; Massudi, R.; Latifi, H., Digital holographic scanning of large objects using a rotating optical slab. *Int. J. Imag. Syst. Tech.* **2006**, *16*, 258-261.
179. Liu, C.; Liu, Z.G.; Bo, F.; Wang, Y.; Zhu, J.Q., Super-resolution digital holographic imaging method. *Appl. Phys. Lett.* **2002**, *81*, 3143-3145.
180. Bianco, V.; Paturzo, M.; Ferraro, P., Spatio-temporal scanning modality for synthesizing interferograms and digital holograms. *Opt.Express* **2014**, *22*, 22328-22339.

181. Mico, V.; Ferreira, C.; Garcia, J., Lensless object scanning holography for two-dimensional mirror-like and diffuse reflective objects. *Appl. Opt.* **2013**, *52*, 6390-6400.
182. Mico, V.; Ferreira, C.; Garcia, J., Surpassing digital holography limits by lensless object scanning holography. *Opt. Express* **2012**, *20*.
183. Binet, R.; Colineau, J.; Lehureau, J.C., Short-range synthetic aperture imaging at 633 nm by digital holography. *Appl. Opt.* **2002**, *41*, 4775-4782.
184. Luo, W.; Greenbaum, A.; Zhang, Y.B.; Ozcan, A., Synthetic aperture-based on-chip microscopy. *Light-Sci Appl.* **2015**, *4*.
185. Zhang, J.L.; Sun, J.S.; Chen, Q.; Li, J.J.; Zuo, C., Adaptive pixel-super-resolved lensfree in-line digital holography for wide-field on-chip microscopy. *Sci Rep.* **2017**, *7*. 11777.
186. Rivenson, Y.; Wu, Y.C.; Wang, H.D.; Zhang, Y.B.; Feizi, A.; Ozcan, A., Sparsity-based multi-height phase recovery in holographic microscopy. *Sci. Rep.* **2016**, *6*. 37862.
187. Greenbaum, A.; Ozcan, A., Maskless imaging of dense samples using pixel super-resolution based multi-height lensfree on-chip microscopy. *Opt. Express* **2012**, *20*, 3129-3143.
188. Wu, Y.C.; Zhang, Y.B.; Luo, W.; Ozcan, A., Demosaiced pixel super-resolution for multiplexed holographic color imaging. *Sci. Rep.* **2016**, 6. 28601.
189. Luo, W.; Zhang, Y.; Feizi, A.; Gorocs, Z.; Ozcan, A., Pixel super-resolution using wavelength scanning. *Light-Sci Appl.* **2016**, *5*.
190. Greenbaum, A.; Luo, W.; Khademhosseinieh, B.; Su, T.W.; Coskun, A.F.; Ozcan, A., Increased space-bandwidth product in pixel super-resolved lensfree on-chip microscopy. *Sci Rep.* **2013**, *3*. 1717.
191. Greenbaum, A.; Feizi, A.; Akbari, N.; Ozcan, A., Wide-field computational color imaging using pixel super-resolved on-chip microscopy. *Opt. Express* **2013**, *21*, 12469-12483.
192. Bishara, W.; Sikora, U.; Mudanyali, O.; Su, T.W.; Yaglidere, O.; Luckhart, S.; Ozcan, A., Holographic pixel super-resolution in portable lensless on-chip microscopy using a fiber-optic array. *Lab. Chip.* **2011**, *11*, 1276-1279.
193. Bishara, W.; Su, T.W.; Coskun, A.F.; Ozcan, A., Lensfree on-chip microscopy over a wide field-of-view using pixel super-resolution. *Opt. Express* **2010**, *18*, 11181-11191.
194. Zheng, G.A.; Lee, S.A.; Yang, S.; Yang, C.H., Sub-pixel resolving optofluidic microscope for on-chip cell imaging. *Lab. Chip.* **2010**, *10*, 3125-3129.
195. Bishara, W.; Zhu, H.Y.; Ozcan, A., Holographic opto-fluidic microscopy. *Opt. Express* **2010**, *18*, 27499-27510.
196. Li, Y.; Lilley, F.; Burton, D.; Lalor, M., Evaluation and benchmarking of a pixel-shifting camera for superresolution lensless digital holography. *Appl. Opt.* **2010**, *49*, 1643-1650.
197. Jacquemod, G.; Odet, C.; Goutte, R., Image-resolution enhancement using subpixel camera displacement. *Signal. Process.* **1992**, *26*, 139-146.
198. Arpali, S.A.; Arpali, C.; Coskun, A.F.; Chiang, H.H.; Ozcan, A., High-throughput screening of large volumes of whole blood using structured illumination and fluorescent on-chip imaging. *Lab. Chip.* **2012**, *12*, 4968-4971.
199. Coskun, A.F.; Sencan, I.; Su, T.W.; Ozcan, A., Lensfree fluorescent on-chip imaging of transgenic caenorhabditis elegans over an ultra-wide field-of-view. *Plos One* **2011**, *6*. e15955.

200. Coskun, A.F.; Sencan, I.; Su, T.W.; Ozcan, A., Lensless wide-field fluorescent imaging on a chip using compressive decoding of sparse objects. *Opt. Express* **2010**, *18*, 10510-10523.
201. Coskun, A.F.; Su, T.W.; Ozcan, A., Wide field-of-view lens-free fluorescent imaging on a chip. *Lab. Chip.* **2010**, *10*, 824-827.
202. Zhang, Y.B.; Wu, Y.C.; Zhang, Y.; Ozcan, A., Color calibration and fusion of lens-free and mobile-phone microscopy images for high-resolution and accurate color reproduction. *Sci. Rep.* **2016**, 6. 27811.
203. Lee, S.A.; Zheng, G.A.; Mukherjee, N.; Yang, C.H., On-chip continuous monitoring of motile microorganisms on an epetri platform. *Lab. Chip.* **2012**, *12*, 2385-2390.
204. Zheng, G.A.; Lee, S.A.; Antebi, Y.; Elowitz, M.B.; Yang, C.H., The epetri dish, an on-chip cell imaging platform based on subpixel perspective sweeping microscopy (spsm). *PNAS* **2011**, *108*, 16889-16894.
205. Joseph, J.; Waldman, D.A., Homogenized fourier transform holographic data storage using phase spatial light modulators and methods for recovery of data from the phase image. *Appl. Opt.* **2006**, *45*, 6374-6380.
206. Rivenson, Y.; Gorocs, Z.; Gunaydin, H.; Zhang, Y.B.; Wang, H.D.; Ozcan, A., Deep learning microscopy. *Optica* **2017**, *4*, 1437-1443.
207. Daloglu, M.U.; Ozcan, A., Computational imaging of sperm locomotion. *Biol. Reprod* **2017**, *97*, 182-188.
208. Su, T.W.; Choi, I.; Feng, J.W.; Huang, K.; McLeod, E.; Ozcan, A., Sperm trajectories form chiral ribbons. *Sci. Rep.* **2013**, 3. 1664.
209. Su, T.W.; Xue, L.; Ozcan, A., High-throughput lensfree 3D tracking of human sperms reveals rare statistics of helical trajectories. *PNAS* **2012**, *109*, 16018-16022.
210. Su, T.W.; Isikman, S.O.; Bishara, W.; Tseng, D.; Erlinger, A.; Ozcan, A., Multi-angle lensless digital holography for depth resolved imaging on a chip. *Opt. Express* **2010**, *18*, 9690-9711.
211. Soldevila, F.; Duran, V.; Clemente, P.; Lancis, J.; Tajahuerce, E., Phase imaging by spatial wavefront sampling. *Optica* **2018**, *5*, 164-174.
212. Gong, H.; Agbana, T.E.; Pozzi, P.; Soloviev, O.; Verhaegen, M.; Vdovin, G., Optical path difference microscopy with a shack-hartmann wavefront sensor. *Opt. Lett.* **2017**, *42*, 2122-2125.
213. Iglesias, I., Pyramid phase microscopy. *Opt. Lett.* **2011**, *36*, 3636-3638.
214. Singh, A.S.G.; Anand, A.; Leitgeb, R.A.; Javidi, B., Lateral shearing digital holographic imaging of small biological specimens. *Opt. Express* **2012**, *20*, 23617-23622.
215. Bon, P.; Maucort, G.; Wattellier, B.; Monneret, S., Quadriwave lateral shearing interferometry for quantitative phase microscopy of living cells. *Opt. Express* **2009**, *17*, 13080-13094.
216. Kemper, B.; Vollmer, A.; Rommel, C.E.; Schnekenburger, J.; von Bally, G., Simplified approach for quantitative digital holographic phase contrast imaging of living cells. *J. Biomed. Opt.* **2011**, *16*.
217. Merola, F.; Miccio, L.; Paturzo, M.; Finizio, A.; Grilli, S.; Ferraro, P., Driving and analysis of micro-objects by digital holographic microscope in microfluidics. *Opt. Lett.* **2011**, *36*, 3079-3081.

218. Fu, D.; Oh, S.; Choi, W.; Yamauchi, T.; Dorn, A.; Yaqoob, Z.; Dasari, R.R.; Feld, M.S., Quantitative dic microscopy using an off-axis self-interference approach. *Opt. Lett.* **2010**, *35*, 2370-2372.
219. Li, Y.; Di, J.L.; Ma, C.J.; Zhang, J.W.; Zhong, J.Z.; Wang, K.Q.; Xi, T.L.; Zhao, J.L., Quantitative phase microscopy for cellular dynamics based on transport of intensity equation. *Opt. Express* **2018**, *26*, 586-593.
220. Zuo, C.; Chen, Q.; Qu, W.J.; Asundi, A., High-speed transport-of-intensity phase microscopy with an electrically tunable lens. *Opt. Express* **2013**, *21*, 24060-24075.
221. Zuo, C.; Chen, Q.; Qu, W.J.; Asundi, A., Noninterferometric single-shot quantitative phase microscopy. *Opt. Lett.* **2013**, *38*, 3538-3541.
222. Kou, S.S.; Waller, L.; Barbastathis, G.; Sheppard, C.J.R., Transport-of-intensity approach to differential interference contrast (ti-dic) microscopy for quantitative phase imaging. *Opt. Lett.* **2010**, *35*, 447-449.
223. Waller, L.; Kou, S.S.; Sheppard, C.J.R.; Barbastathis, G., Phase from chromatic aberrations. *Opt. Express* **2010**, *18*, 22817-22825.
224. Camacho, L.; Mico, V.; Zalevsky, Z.; Garcia, J., Quantitative phase microscopy using defocusing by means of a spatial light modulator. *Optics Express* **2010**, *18*, 6755-6766.
225. Barty, A.; Nugent, K.A.; Paganin, D.; Roberts, A., Quantitative optical phase microscopy. *Opt. Lett.* **1998**, *23*, 817-819.
226. Bao, P.; Zhang, F.C.; Pedrini, G.; Osten, W., Phase retrieval using multiple illumination wavelengths. *Opt. Lett.* **2008**, *33*, 309-311.
227. Gao, P.; Pedrini, G.; Zuo, C.; Osten, W., Phase retrieval using spatially modulated illumination. *Opt. Lett.* **2014**, *39*, 3615-3618.
228. Lee, D.J.; Han, K.; Lee, H.J.; Weiner, A.M., Synthetic aperture microscopy based on referenceless phase retrieval with an electrically tunable lens. *Appl. Opt.* **2015**, *54*, 5346-5352.
229. Barty, A.; Nugent, K.A.; Paganin, D.; Roberts, A., Quantitative optical phase microscopy. *Opt. Lett.* **1998**, *23*, 817-819.
230. Yang, T.D.; Kim, H.J.; Lee, K.J.; Kim, B.M.; Choi, Y., Single-shot and phase-shifting digital holographic microscopy using a 2-d grating. *Opt. Express* **2016**, *24*, 9480-9488.
231. Mico, V.; Ferreira, C.; Zalevsky, Z.; Garcia, J., Spatially-multiplexed interferometric microscopy (smim): Converting a standard microscope into a holographic one. *Opt.Express* **2014**, *22*, 14929-14943.
232. Picazo-Bueno, J.A.; Zalevsky, Z.; Garcia, J.; Ferreira, C.; Mico, V., Spatially multiplexed interferometric microscopy with partially coherent illumination. *J. Biomed. Opt.* **2016**, *21*.
233. Liu, J.; Li, Y.; Wang, W.B.; Zhang, H.; Wang, Y.H.; Tan, J.B.; Liu, C.G., Stable and robust frequency domain position compensation strategy for fourier ptychographic microscopy. *Opt. Express* **2017**, *25*, 28053-28067.
234. Chung, J.; Lu, H.W.; Ou, X.Z.; Zhou, H.J.; Yang, C.H., Wide-field fourier ptychographic microscopy using laser illumination source. *Biomed. Opt. Express* **2016**, *7*, 4787-4802.
235. Ou, X.Z.; Horstmeyer, R.; Zheng, G.A.; Yang, C.H., High numerical aperture fourier ptychography: Principle, implementation and characterization. *Opt. Express* **2015**, *23*, 3472-3491.

236. Ou, X.Z.; Horstmeyer, R.; Yang, C.H.; Zheng, G.A., Quantitative phase imaging via fourier ptychographic microscopy. *Opt. Lett.* **2013**, *38*, 4845-4848.
237. Zheng, G.A.; Horstmeyer, R.; Yang, C.H., Wide-field, high-resolution fourier ptychographic microscopy. *Nat. Photon.* **2013**, *7*, 739-745.
238. Tian, L.; Liu, Z.J.; Yeh, L.H.; Chen, M.; Zhong, J.S.; Waller, L., Computational illumination for high-speed in vitro fourier ptychographic microscopy. *Optica* **2015**, *2*, 904-911.
239. He, X.L.; Liu, C.; Zhu, J.Q., Single-shot fourier ptychography based on diffractive beam splitting. *Opt. Lett.* **2018**, *43*, 214-217.
240. Sun, J.S.; Zuo, C.; Zhang, L.; Chen, Q., Resolution-enhanced fourier ptychographic microscopy based on high-numerical-aperture illuminations. *Sci. Rep.* **2017**, 7. 1187.
241. Zuo, C.; Sun, J.S.; Li, J.J.; Zhang, J.L.; Asundi, A.; Chen, Q., High-resolution transport-of-intensity quantitative phase microscopy with annular illumination. *Sci. Rep.* **2017**, *7*. 7654.
242. Tian, L.; Wang, J.Y.; Waller, L., 3D differential phase-contrast microscopy with computational illumination using an led array. *Opt. Lett.* **2014**, *39*, 1326-1329.
243. Horstmeyer, R.; Heintzmann, R.; Popescu, G.; Waller, L.; Yang, C.H., Standardizing the resolution claims for coherent microscopy. *Nat. Photon.* **2016**, *10*, 68-71.
244. Zalevsky, Z.; Mendlovic, D., Optical super resolution. *Springer* **2002**.
245. Wolbarsh.Ml, Born,m - Principles of Optics. *Q. Rev. Biol.* **1966**, *41*, 440-&.